Since January 2020 Elsevier has created a COVID-19 resource centre with free information in English and Mandarin on the novel coronavirus COVID-19. The COVID-19 resource centre is hosted on Elsevier Connect, the company's public news and information website.

Elsevier hereby grants permission to make all its COVID-19-related research that is available on the COVID-19 resource centre - including this research content - immediately available in PubMed Central and other publicly funded repositories, such as the WHO COVID database with rights for unrestricted research re-use and analyses in any form or by any means with acknowledgement of the original source. These permissions are granted for free by Elsevier for as long as the COVID-19 resource centre remains active.

Bioorganic Chemistry 115 (2021) 105196

Contents lists available at ScienceDirect

Bioorganic Chemistry

journal homepage: www.elsevier.com/locate/bioorg

Discovery and evolution of 12*N*-substituted aloperine derivatives as anti-SARS-CoV-2 agents through targeting late entry stage

Kun Wang [a,1], Jia–Jing Wu [b,1], Xin–Zhang [a], Qing–Xuan Zeng [a], Na Zhang [a], Wei–Jin Huang [b], Sheng Tang [a], Yan–Xiang Wang [a], Wei–Jia Kong [a], You–Chun Wang [b], Ying–Hong Li [a,c,**], Dan–Qing Song [a,*]

[a] *Beijing Key Laboratory of Antimicrobial Agents, Institute of Medicinal Biotechnology, Chinese Academy of Medical Sciences & Peking Union Medical College, Beijing 100050, China*

[b] *Division of HIV/AIDS and Sex-Transmitted Virus Vaccines, Institute for Biological Product Control, National Institutes for Food and Drug Control (NIFDC) and WHO Collaborating Center for Standardization and Evaluation of Biologicals, Beijing 102629, China*

[c] *State Key Laboratory of Bioactive Substance & Functions of Natural Medicines, Institute of Materia Medica, Chinese Academy of Medical Sciences & Peking Union Medical College, Beijing 100050, China*

ARTICLE INFO

Keyword:
COVID-19
Aloperine
SARS-CoV-2
Cathepsin B
Cytokine

ABSTRACT

So far, there is still no specific drug against COVID-19. Taking compound **1** with anti-EBOV activity as the lead, fifty-four 12*N*-substituted aloperine derivatives were synthesized and evaluated for the anti-SARS-CoV-2 activities using pseudotyped virus model. Among them, **8a** exhibited the most potential effects against both pseudotyped and authentic SARS-CoV-2, as well as SARS-CoV and MERS-CoV, indicating a broad-spectrum anti-coronavirus profile. The mechanism study disclosed that **8a** might block a late stage of viral entry, mainly via inhibiting host cathepsin B activity rather than directly targeting cathepsin B protein. Also, **8a** could significantly reduce the release of multiple inflammatory cytokines in a time- and dose-dependent manner, such as IL-6, IL-1β, IL-8 and MCP-1, the major contributors to cytokine storm. Therefore, **8a** is a promising agent with the advantages of broad-spectrum anti-coronavirus and anti-cytokine effects, thus worthy of further investigation.

1. Introduction

Up to now, the Coronavirus Disease 2019 (COVID-19) epidemic caused by severe acute respiratory syndrome coronavirus 2 (SARS-CoV-2) is still spreading around the world and has yet to be effectively controlled [1,2], and SARS-CoV-2 is little known to us. Though several promising small molecule candidates had been used in clinic, such as RNA-dependent RNA polymerase inhibitor remdesivir [3,4] and anti-malarial hydroxychloroquine (Fig. 1) [5,6], none of them showed satisfactory clinical effects [7–13]. In October 2020, remdesivir was approved by FDA for the treatment of COVID-19 patients in hospital [14]. However, with the emergence of the mutation of SARS-CoV-2 strains such as D614G and recurrent COVID-19 pneumonia, the treatment of COVID-19 is becoming more and more complicated and difficult [15–19]. Thus, it is of great significance to find broad-spectrum anti-SARS-CoV-2 drugs that are not affected by virus variation and drug resistance.

Cytokine storm is one of the leading causes of death in patients with severe and critically ill COVID-19 [20,21], with significantly increased proinflammatory cytokine levels in patients, including interleukin (IL)-6, IL-1β, IL-2, IL-8, MCP-1 and tumour necrosis factor alpha (TNFα). However, both highly specific IL-6/IL-6R antibodies tocilizumab and sarilumab failed in the treatment of patients with severe or critically ill COVID-19 in phase III clinical trials. Meantime, dexamethasone (Fig. 1), a broad-spectrum immunosuppressive agent, effectively reduced mortality in critically ill patients [22], indicating the advantage of inhibiting multiple cytokines over inhibiting a single cytokine. Therefore, it is imperative to discover broad-spectrum anti-coronavirus and anti-cytokine agents to effectively prevent and control COVID-19 and cytokine storm syndrome.

* Corresponding author.
** Corresponding author at: Beijing Key Laboratory of Antimicrobial Agents, Institute of Medicinal Biotechnology, Chinese Academy of Medical Sciences & Peking Union Medical College, Beijing 100050, China.
E-mail addresses: liyinghong@imb.pumc.edu.cn (Y. Li), songdanqing@imb.pumc.edu.cn (D. Song).
[1] These authors made equal contribution to this work.

https://doi.org/10.1016/j.bioorg.2021.105196
Received 12 January 2021; Received in revised form 16 July 2021; Accepted 18 July 2021
Available online 22 July 2021
0045-2068/© 2021 Elsevier Inc. All rights reserved.

In recent years, our team has been committed to the discovery of novel antiviral candidates from Tradition Chinese Medicine such as *Sophora alopecuroides* [23–25]. Earlier, our team found that 12*N*-3′,4′-dichlorobenzyl aloperine (**1**, Fig. 2) with a unique endocyclic skeleton had a broad-spectrum anti-filovirus effect against both Ebola virus (EBOV) and Marburg virus (MARV) with EC_{50} of 4.8 and 7.1 μM respectively, via targeting lysosome cathepsin B (Cat B) of host cells [23,26,27]. These results provoked us to further test its activity against SARS-CoV-2 using the newly constructed SARS-CoV-2 pseudotyped virus model in our lab [28,29]. As anticipated, compound **1** exhibited a moderate activity against SARS-CoV-2 with an EC_{50} value of 28.2 μM and a selectivity index (SI) value of 5.2, showing an ideal lead for further structure modification and optimization for SARS-CoV-2.

Therefore, as showed in Fig. 2, taking compound **1** as the lead, several series of 12*N*-substituted aloperine derivatives were synthesized and evaluated for their anti-SARS-CoV-2 activity using pseudotyped virus model. Furthermore, the structure–activity relationship (SAR) analysis, anti-coronavirus and anti-cytokine effects, as well as pharmacokinetics (PK), safety profiles and primary mechanism exploration of key compounds were carried out in this study.

2. Results and discussion

2.1. Chemistry

A total of 54 12*N*-substituted aloperine derivatives, of which 39 were new, were prepared from commercially available aloperine with purity over 95%, which was purchased from Yanchi Dushun Biological and Chemical Co. Ltd. (Shanxi, China). The synthesis route of all the target compounds is displayed in Scheme 1. Among all the target compounds, 12*N*-benzyl (**2a**–**e**), 12*N*-benzoyl (**3a**–**c**), 12*N*-sulfonyl (**4a**–**c**), 12*N*-alkyl (**8a**, **8b**), 12*N*-carbamoylmethyl (**11l**, **11s**) aloperine derivatives have been reported previously in our lab [23,30], and the rest are newly synthesized ones.

Various substituted amines (**9a**–**s**) were respectively acylated with bromoacetyl bromide to yield key intermediates **10a**–**s**, which underwent an *N*-alkylation reaction with aloperine to get target compounds **11a**–**s** in total yields of 11–53%. Another series of target compounds **14a**–**r** was respectively gained through a condensation reaction of aloperine and the key intermediates **13a**–**r**, which were prepared via an alkylation of commercially available different substituted amines **12a**–**r** and ethyl bromoacetate, followed by an ester hydrolysis with LiOH as the base. The third series of products **15a**–**d** were respectively obtained through a nucleophilic addition reaction between aloperine and isocyanates in equal molar ratio in 26–63% yields. All the final products were purified by flash column chromatography on silica gel with CH_2Cl_2/CH_3OH as the gradient eluent.

2.2. Biological activity evaluation

2.2.1. SAR analysis for anti-SARS-CoV-2 activity

As reported earlier, the SARS-CoV-2 pseudovirus model was composed of plasmid pcDNA3.1.S2 expressing the key spike (S) protein and vesicular stomatitis virus (VSV) G pseudotyped virus (G*ΔG-VSV) that packages expression cassettes for firefly luciferase instead of VSV-G in the VSV genome [28]. The VSV G pseudovirus was then applied to identify their anti-VSV effects as a comparison, and inhibition of SARS-CoV-2 infection was detected as a decrease in luciferase signal. The structures, antivirus activity and cytotoxicity of all the 54 target compounds against SARS-CoV-2 and VSV were shown in Table 1. The anti-SARS-CoV-2 potency of each compound was evaluated by the combination of its EC_{50} and SI values as the important evaluation indication, while referring to the EC_{50} of VSV.

SAR study was mainly focused on the influence of substituents on the 12-nitrogen atom, taking **1** with a 3, 4-dichlorobenzyl substituent as the lead. First, the methylene linker was retained, a series of 12*N*-benzyl aloperine derivatives **2a**–**e** was synthesized and evaluated. Compounds **2a**–**d** gave significantly decreased potency, while compound **2e** with a 2, 4-dichlorobenzyl exhibited a moderate activity with EC_{50} of 22.0 μM, comparable potency to **1**. Then, the mono- or dichlorophenyl was retained, and the replacement of methylene linker with carbonyl or sulfonyl yielded compounds **3a**–**c** and **4a**–**c**, which decreased activity in varying degrees. Furthermore, the extension of methylene to dimethylene and trimethylene gave compounds **8a** and **8b**, which exhibited promising potencies with EC_{50} values of 19.1 and 7.4 μM and SI values of over 14.0 and 7.9, respectively, indicating that the change of the linker might benefit the activity.

Next, methylene linker was replaced by carbamoylmethyl while a mono- or di-halophenyl element was retained, by which compounds **11a**–**g** were invented and evaluated. As shown in Table 1, all of them displayed the declined activities to varying degrees, regardless of mono- or dihalophenyl substitution. Meanwhile, a halogen atom along with methyl, trifluoromethyl or trifluoromethoxy was introduced on the benzene ring to form compounds **11h**–**m**, and most of them gave declined activities except that **11k** and **11m** gave slightly elevated activity. In addition, the introduction of dimethylphenyl, ditrifluoromethylphenyl, or bulky naphthyl, quinolyl and tertiary amine moiety in compounds **11n**–**s**, caused a decrease in activity. Finally, the methylene linker was changed into aminoacetyl or carbamoyl linker to achieve compounds **14a**–**r** and **15a**–**d**, respectively. Most of them displayed comparable or decreased activity compared to the lead **1**, except that compound **14f** bearing the iodophenyl exhibited an elevated activity with the EC_{50} value of 9.4 μM and SI values of 11.4, indicating that iodine or chlorine atom on the phenyl ring might be beneficial for the activity.

In addition, as showed in Table 1, most of the target compounds also exhibited varying degrees of activity to VSV skeleton, therefore the antiviral activity against authentic SARS-CoV-2 should be conducted to exclude the active compounds through anti-VSV pathway for anti-SARS-CoV-2 effects.

2.2.2. Antiviral evaluation of compounds *2e, 8a* and *8b* against coronaviruses

The active compounds **2e**, **8a** and **8b** bearing a common chlorobenzene were chosen to test their antiviral activities against authentic SARS-CoV-2 in Vero E6 cells in a BSL-3 lab. As displayed in Table 2, compounds **2e** and **8b** had no activity against authentic SARS-CoV-2, indicating that the anti-SARS-CoV-2 activity in pseudovirus model might be from anti-VSV; while compound **8a** displayed a moderate activity against authentic SARS-CoV-2 with an EC_{50} value of 39.1 μM and SI value of > 6.8, basically consistent with those in the pseudovirus model.

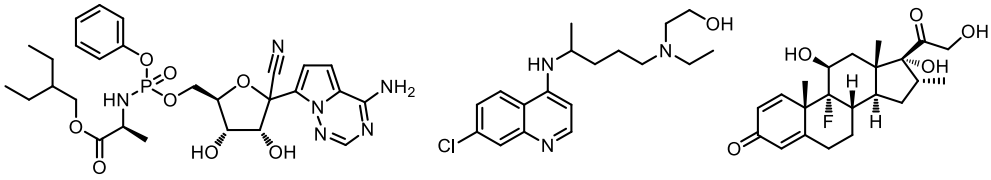

Fig. 1. Structures of remdesivir (left), hydroxychloroquine (center) and dexamethasone (right).

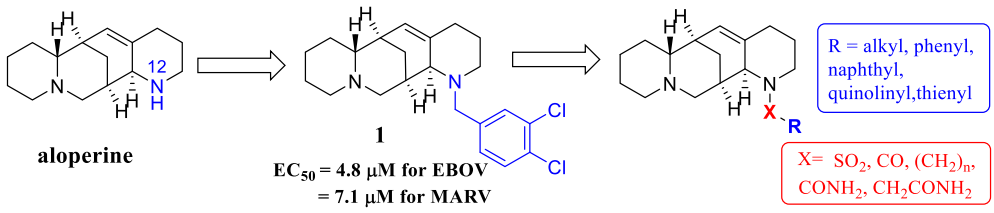

Fig. 2. Chemical structures of aloperine and lead **1** as well as modification strategies.

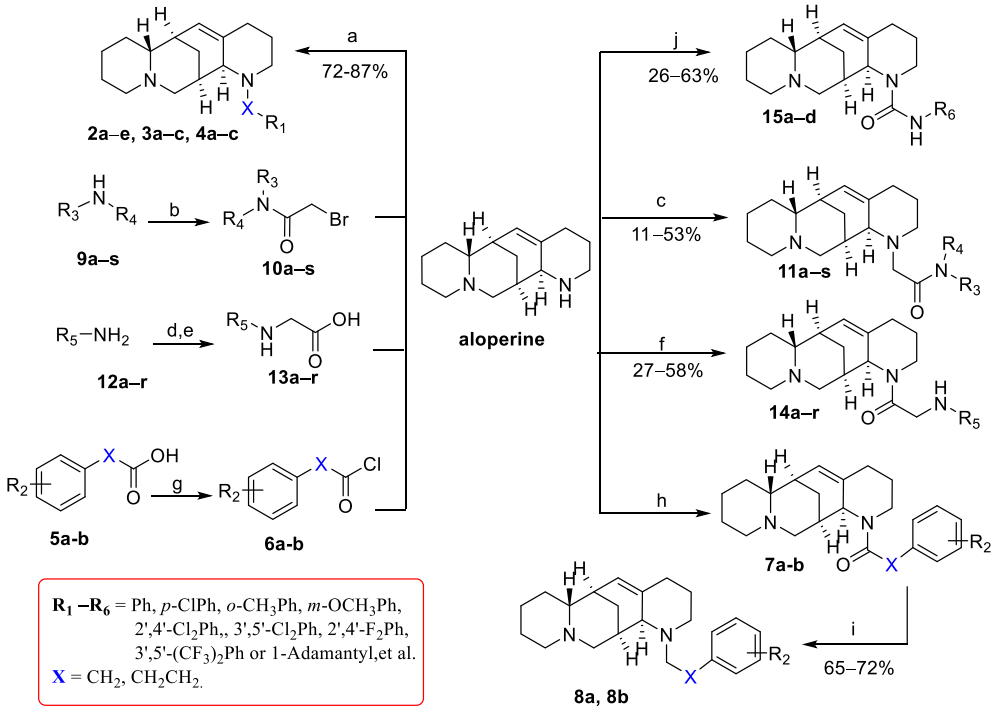

Scheme 1. (a) R_1XBr and R_1XCl, MeCN or CH_2Cl_2, K_2CO_3, r.t., 2 h; (b) bromoacetyl bromide, CH_2Cl_2, Et_3N, 0 °C to r.t., 2 h; (c) CH_2Cl_2, Et_3N, r.t.; (d) ethyl bromoacetate, EtOH/$NaHCO_3$, reflux, 8 h; (e) LiOH, H_2O, reflux 1.5 h; (f) HOBt, DIEA, EDCI, CH_2Cl_2, 0 °C to r.t.; (g) $SOCl_2$, reflux, 2 h; (h) K_2CO_3, CH_2Cl_2, r.t., 2 h; (i) $LiAlH_4$, THF, r.t., 2 h; (j) R_6NCO, CH_2Cl_2, Et_3N, 0 °C to r.t., 1 h.

To further evaluate the broad-spectrum anti-coronavirus effect of compound **8a**, SARS-CoV and Middle East respiratory syndrome coronavirus (MERS-CoV) pseudovirus models were applied herein [31]. As displayed in the Table 2, **8a** showed better activity against SARS-CoV and MERS-CoV, indicating their broad-spectrum anti-coronavirus potential. As anticipated, **8a** exhibited the higher anti-SARS-CoV and anti-MERS-CoV activity with EC_{50} values of 5.6 and 9.4 μM, respectively, and thus was selected as a representative compound for the next step.

2.3. Compound *8a* blocks the late stage of SARS-CoV-2 entry

The SARS-CoV-2 pseudovirus model was virtually replication-defective VSV particles incorporated with the S protein of SARS-CoV-2, which could reflect only a few key steps in the entry into host cells. SARS-CoV-2 entry into host cells can be divided into several steps, including binding to angiotensin-converting enzyme 2 (ACE2) receptor on cell surface, entering host cell through endocytosis, and releasing the fuse peptide to fuse viral and lysosomal membranes [32–36]. Any step in the process of entry is blocked to prevent infections. Therefore, a single-cycle time-of-addition experiment was initially performed on our SARS-CoV-2 pseudovirus model to determine the specific blockage stage of compound **8a** in SARS-CoV-2 entry, via adding **8a** and pseudovirus at different time points and incubation temperature, as depicted in Fig. 3A.

As shown in Fig. 3B, compound **8a** had an inhibition rate of 27% on process **a**, but no inhibitory activity on process **b** and **c**, showing a weak or no inhibitory effect on the early stage of virus entry. Meanwhile, compound **8a** showed a higher inhibition rate of 76% on process **d**, suggesting that compound **8a** might affect membrane fusion process at late entry stage of SARS-CoV-2 infection, consistent with those of lead compound **1** against EBOV and MARV, mainly via inhibiting endosomal cysteine protease Cat B activity [23,25].

2.4. Compound *8a* inhibits Cat B activity in host cells

Considering the critical role of host Cat B and Cat L in membrane fusion of SARS-CoV-2 and similar mechanism of action of aloperine analogue **1,** the inhibition activity of compound **8a** on Cat B and Cat L enzyme in Huh 7 cells were evaluated respectively [37]. As displayed in Fig. 4A and 4B, compound **8a** significantly inhibited the Cat B activity with an IC_{50} value of 9.9 μM, but had no effect on Cat L. Furthermore, the affinity between **8a** and recombinant Cat B was also measured to identify its direct binding with Cat B. However, as shown in Fig. 4C, compound **8a** had a poor affinity with Cat B, indicating that **8a** exerted a broad-spectrum anti-coronavirus effect, mainly via inhibiting host Cat B activity, rather than directly targeting Cat B protein.

In order to further confirm that Cat B is necessary for SARS-CoV-2 entry into the host cells, we selected a specific Cat B inhibitor CA-074 with a Ki value of 2–5 nM to test its anti-SARS-CoV-2 activity in pseudovirus model. As shown in Table 1, compound CA-074 exhibited a good potency with an EC_{50} value of 2.7 μM against SARS-CoV-2, and only

Table 1
Structures and antiviral activities of all the target compounds against SARS-CoV-2.

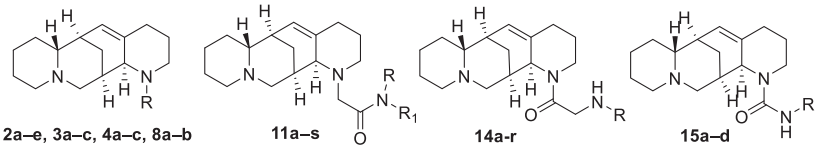

2a–e, 3a–c, 4a–c, 8a–b **11a–s** **14a-r** **15a–d**

No	R	R_1	CC_{50}(μM)[a]	EC_{50}-SARS- CoV-2(μM)[b]	SI[c]	EC_{50}-VSV (μM)
1	3′,4′-Cl_2PhCH_2	/	147.3	28.2	5.2	15.9
2a	PhCH_2	/	>266.7	162.6	>1.6	68.9
2b	*p*-ClPhCH_2	/	>266.7	115.5	>2.3	40.2
2c	*o*-CH_3PhCH_2	/	>266.7	97.0	>2.7	25.4
2d	*m*-OCH_3PhCH_2	/	>266.7	151.5	>1.8	15.9
2e	2′,4′-Cl_2PhCH_2	/	138.0	22.0	6.3	16.2
3a	*p*-ClPhCO	/	>266.7	235.6	–	214.4
3b	3′,4′-Cl_2PhCO	/	>266.7	196.9	–	48.7
3c	3′,5′-Cl_2PhCO	/	170.3	65.6	2.6	79.2
4a	*p*-ClPhSO_2	/	>266.7	>266.7	–	267.6
4b	3′,4′-Cl_2PhSO_2	/	>266.7	136.8	>1.9	175.6
4c	3′,5′-Cl_2PhSO_2	/	>266.7	49.0	>5.4	38.5
8a	*p*-ClPh$(CH_2)_2$	/	>266.7	19.1	>14.0	25.9
8b	3′,5′-Cl_2Ph$(CH_2)_3$	/	58.1	7.4	7.9	6.9
11a	*p*-ClPh	H	>266.7	103.2	>2.6	154.6
11b	*p*-BrPh	H	>266.7	62.8	>4.2	79.9
11c	*p*-IPh	H	124.4	29.5	4.2	47.8
11d	2′,4′-Cl_2Ph	H	167.4	54.8	3.1	70.5
11e	2′,5′-Br_2Ph	H	163.9	55.3	3.0	40.3
11f	2′-F-5′-BrPh	H	221.8	57.5	3.9	66.8
11g	2′-Cl-5′-BrPh	H	>266.7	90.3	>3.0	77.5
11h	2′-F-6′-CH_3Ph	H	>266.7	>266.7	–	>266.7
11i	2′-Cl-4′-CH_3Ph	H	>266.7	77.4	>3.4	87.9
11j	2′–CH_3-4′-ClPh	H	>266.7	106.8	>2.5	75.1
11k	3′-Cl-5′-CF_3Ph	H	57.1	10.4	5.5	17.5
11l	3′-Cl-5′-CF_3OPh	H	62.8	14.7	4.3	21.8
11m	3′-CF_3-4′-BrPh	H	38.3	4.0	9.6	6.0
11n	3′,4′-$(CH_3)_2$Ph	H	>266.7	70.8	>3.8	107.7
11o	3′,5′-$(CF_3)_2$Ph	H	71.0	17.0	4.2	21.9
11p		H	96.7	37.1	2.6	43.5
11q		H	>266.7	67.4	>4.0	119.8
11r	*p*-BrPh	CH_3	>266.7	42.3	>6.3	152.9
11s		Ph	45.1	10.8	4.2	14.2
14a	Ph	H	>266.7	>266.7	–	>266.7
14b	*p*-FPh	H	>266.7	177.4	>1.5	>266.7
14c	*m*-FPh	H	>266.7	144.4	>1.8	>266.7
14d	*p*-ClPh	H	>266.7	61.3	>4.4	162.8
14e	*p*-BrPh	H	180.1	37.3	4.8	85.4
14f	*p*-IPh	H	106.8	9.4	11.4	50.2
14g	*p*-CH_3Ph	H	>266.7	>266.7	–	>266.7
14h	*m*-CF_3Ph	H	>266.7	69.2	>3.9	134.1
14i	*m*-CH_3OPh	H	>266.7	>266.7	–	>266.7
14j	*p*-CF_3OPh	H	117.6	19.3	6.1	47.6
14k	2′,4′-Cl_2Ph	H	65.8	17.8	3.7	36.2
14l	3′,4′-Cl_2Ph	H	63.0	15.8	4.0	35.9
14m	3′,5′-$(CH_3)_2$Ph	H	>266.7	>266.7	–	>266.7
14n	3′,5′-$(CH_3O)_2$Ph	H	>266.7	>266.7	–	>266.7
14o	3′,5′-$(CF_3)_2$Ph	H	112.7	37.6	3.0	48.3
14p		H	199.1	73.6	2.7	124.6
14q		H	224.1	87.2	2.6	108.3
14r	*p*-ClPh	CH_3	191.8	21.1	9.1	85.6
15a	2′,4′-F_2Ph	H	>266.7	195.4	>1.4	138.6
15b	3′,5′-$(CH_3)_2$Ph	H	>266.7	151.4	>1.8	94.9
15c	3′,5′-$(CF_3)_2$Ph	H	53.9	11.5	4.7	14.9
15d		H	>266.7	52.9	>5.0	106.7
CA-074	/	/	230.7	2.7	85.4	10.5

[a] The concentration of 50% cellular toxicity in Huh 7 cells.
[b] The concentration of compound that inhibited 50% of the virus level in Huh 7 cells.
[c] The selectivity index-the ratio of CC_{50} to EC_{50}.

Table 2
Antiviral activities of part compounds against different coronaviruses.

No	CC_{50} (μM)[a]	EC_{50}(μM)				
		Authentic SARS-CoV-2[b]	Pseudo SARS-CoV-2[c]	Pseudo SARS-CoV[c]	Pseudo MERS-CoV[c]	Pseudo VSV[c]
2e	177.4	>3750	22.0	NT[d]	NT[d]	16.2
8a	>266.7	39.1	19.1	5.6	9.4	25.9
8b	109.6	>3750	7.4	NT[d]	NT[d]	6.9

[a] CC_{50}: the concentration of 50% cellular toxicity in Vero E6 cell;
[b] EC_{50}: the concentration of compound that inhibited 50% of the virus level in Vero E6 cell.
[c] EC_{50}: the concentration of compound that inhibited 50% of the virus level in Huh 7 cell.
[d] NT: not tested.

moderate activity against VSV with an EC_{50} value of 10.5 μM, indicating that CA-074 could selectively inhibit SARS-CoV-2 activity. Then, the time-of-addition experiment of CA-074 was conducted, as depicted in Fig. 3C. Compound CA-074 significantly inhibited **a**, **b** and **d** stages with inhibitory rates of 87%, 77% and 93%, respectively, indicating a multi-target mechanism of action, in which the inhibition of Cat B in process **d** plays an important role. These results suggested that Cat B might be an ideal target for anti-SARS-CoV-2 drugs.

2.5. Inhibitory effects on cytokines of compound *8a*

To further understand the inhibitory effects of **8a** on the secretion of multiple proinflammatory factors, four cytokines including IL-6, IL-1β, IL-8, and MCP-1 were analyzed in phorbol 12-myristate 13-acetate-differentiated human monocytic cell line-1 (PMA-THP-1) triggered by lipopolysaccharide (LPS) plus nigericin (Nig) using ELISA assay [38].

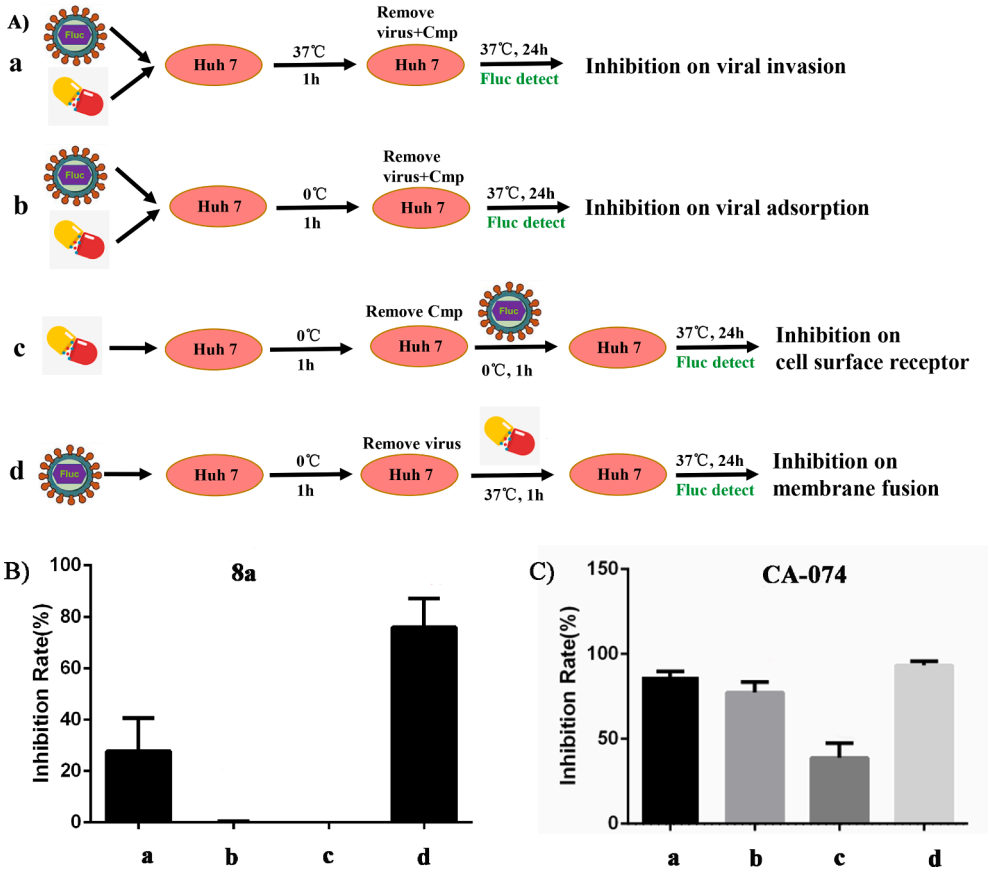

Fig. 3. Compounds 8a and CA-074 block SARS-CoV-2 entry into host cells. (A) Cartoon diagram of a single-cycle time-of-addition at different time and temperature. (B) Compound **8a** and (C) CA-074 block SARS-CoV-2 infection at different entry stage. Error bars indicate standard deviations.

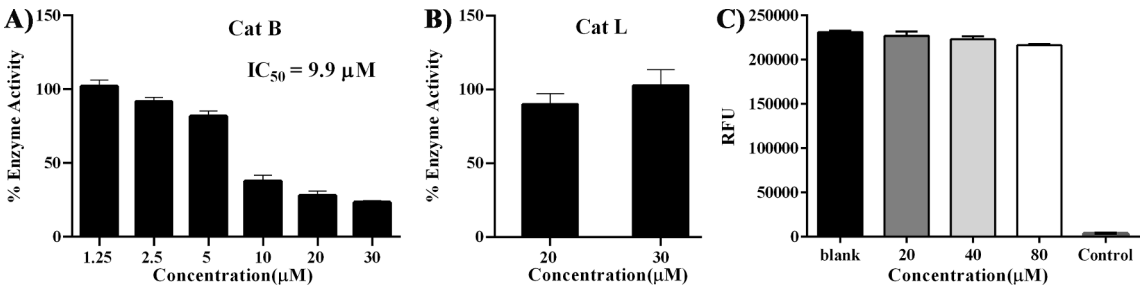

Fig. 4. Effects of 8a on Cat B and Cat L. (A) Inhibitory activity of **8a** Cat B in Huh 7 cells. (B) Inhibitory activity of **8a** Cat L. (C) Affinity activity of **8a** to recombinant Cat B.

Cells were primed with LPS (1 μg/mL) and then stimulated with Nig (5 μM) without or with **8a** pre-treatment for different concentrations (5, 10 or 20 μM) and for different time (3 h, 6 h, 12 h or 24 h). As shown in Fig. 5, compound **8a** significantly reduced the releases of IL-6, IL-1β, IL-8 and MCP-1 in a dose-dependent and time-dependent manner, suggesting a broad-spectrum inhibiting activity of multiple cytokines.

2.6. PK and safety profiles of *8a* in vivo

The *in vivo* PK behavior of compound **8a** was evaluated in SD rat via oral administration at the dosage of 25 mg/kg. As showed in Table 3, compound **8a** gave the good *in vivo* PK parameters with a maximum plasma concentration (C_{max}) value of 0.82 μM, a half-life ($T_{1/2}$) of 2.5 h and an area under the curve (AUC) value of 4.47 μM·h, suggesting an ideal PK profile of compound **8a**.

Next, the acute toxicity assessment of **8a** was performed in Kunming mice in a single oral administration at the dosage of 0, 250, 500 or 1000 $mg{\cdot}kg^{-1}$ respectively. The mice were closely monitored for 7 days. The results demonstrated that the oral median lethal dose (LD_{50}) value of compound **8a** was 812 mg/kg. At the end of the experiment, blood samples of 250 and 500 mg/kg groups were respectively taken for liver and kidney function measurement. As displayed in Fig. 6, significant abnormality was not found in aminotransferase (AST) and alanine aminotransferase (ALT), as well as blood urea nitrogen (BUN) and serum creatinine (SCR) levels, indicating no toxicity to the liver or kidney function, and therefore a good oral safety profile of compound **8a**.

3. Conclusions

In summary, 54 aloperine derivatives with a unique endocyclic scaffold, of which 39 were new, were synthesized and evaluated for their anti-SARS-CoV-2 activities on a pseudotyped virus model. Among them, compound **8a** with a 12*N*-*p*-chlorophenyl moiety exhibited the broad-spectrum anti-coronavirus effects against both pseudotyped and authentic SARS-CoV-2, as well as SARS-CoV and MERS-CoV, through targeting host cell components. It might block viral entry at a late stage by inhibiting host Cat B activity, which has the advantage of not being affected by virus mutation and drug resistance. Meanwhile, **8a** could significantly reduce the levels of multiple inflammatory cytokines including IL-6, IL-1β, IL-8 and MCP-1 in a dose- and time-dependent manner. Furthermore, compound **8a** showed a good PK and safety profile *in vivo*, suggesting an ideal drug-like feature. Therefore, aloperine derivative **8a** has the advantage of broad-spectrum anti-coronavirus and anti-cytokine activity in the treatment of COVID-19, which is worth further investigation.

Table 3
The oral PK and safety profile of compound **8a**.

No	T_{max} (h)	C_{max} (μM)	AUC_{0-t} (μM·h)	$AUC_{0-\infty}$ (μM·h)	MRT (h)	$t_{1/2}$ (h)	LD_{50} (mg/kg)
8a	2.50 ± 3.04	0.82 ± 0.32	4.47 ± 0.95	4.85 ± 0.26	4.59 ± 1.29	2.90 ± 1.69	812

AUC: Area under the concentration–time curve; C_{max}: Maximum plasma concentration; MRT: Mean residence time; T_{max}: peak time; $T_{1/2}$: Half-life; LD_{50}: 50% lethal dose.

4. Experimental section

4.1. Apparatus, materials, and analysis reagents

All commercial solvents and reagents were used without any purification. All reactions were monitored by thin layer chromatography (TLC) and visualized under UV light at 254 nm or iodine fumigation. Melting points (mp) were obtained with a MP90 melting point apparatus (Mettler-Toledo, Greifensee, Switzerland). ^{1}H and ^{13}C NMR spectral

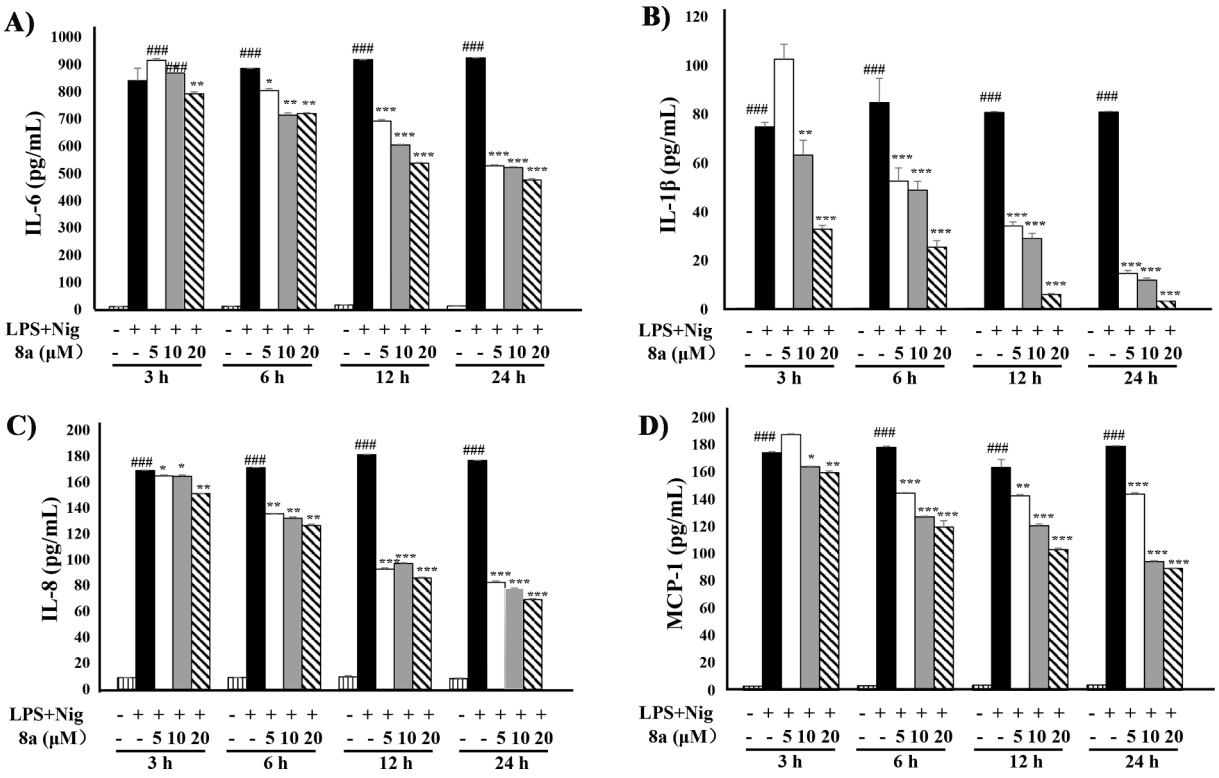

Fig. 5. Compound 8a inhibits releases of cytokines. (A) IL-6, (B) IL-1β, (C) IL-8 and (D) MCP-1 in a concentration-dependent and time-dependent manner. Data were presented as the mean ± SEM, (###) $p < 0.001$ as compared to that of control group; (*) $p < 0.05$, (**) $p < 0.01$ (***) $p < 0.01$ as compared to that of LPS/Nig group. The experiment was repeated for 3 times.

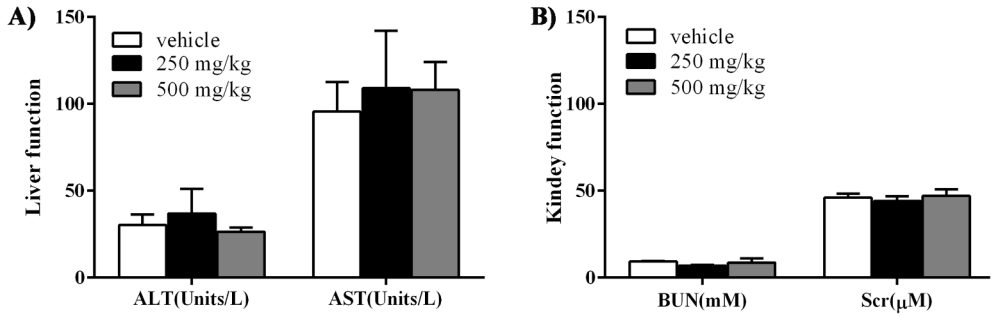

Fig. 6. Effects of compound 8a on liver or kidney function in Kunming mice. (A) ALT and AST levels, (B) BUN and Scr levels in the treatment of **8a** at the dosage of 250 or 500 mg/kg were tested. Data were presented as mean and sd values.

data were recorded with a Bruker Avance 400, 500 or 600 spectrometers (Varian, San Francisco, USA) in DMSO-d_6 or $CDCl_3$ using tetramethylsilane (TMS) as the internal standard. High-resolution mass spectrometry (HRMS) was performed on an AutospecUitima-TOF mass spectrometer (Micromass UK Ltd., Manchester, U.K.). The flash column chromatograms were conducted on silica gel (200–300 mesh) using Combiflash Rf 200 (Teledyne, NE, USA).

4.2. Chemistry

4.2.1. General procedure for the synthesis of the reported compounds

The synthetic methods and structural identification of compounds **2a**–**e**, **3a**–**c**, **4a**–**c**, **8a**, **8b**, **11l** and **11s** have been previously reported in our lab [23,30].

4.2.2. General procedure for the synthesis of 12N-carbamoylmethyl aloperines (*11a*–*s*)

Bromoacetyl bromide (0.4 g, 2 mmol) was added dropwise to a mixture of the different amines **9a**–**s** (2 mmol) and triethylamine (0.3 mL, 2 mmol) in anhydrous CH_2Cl_2 (30 mL) in ice bath, and the mixture was stirred for 30 min at 0 °C and stirred at r.t. for another 1.5 h until TLC indicated complete reaction. Then, triethylamine (0.3 mL, 2 mmol) and aloperine (0.5 g, 2 mmol) were added and the mixture was stirred overnight at r.t. till the TLC showed completion of the reaction. The mixture was then washed with water (20 mL) and brine (20 mL), dried over anhydrous Na_2SO_4, filtered and concentrated to dryness. The residue was purified by flash column chromatography with CH_2Cl_2/CH_3OH to give the target compounds **11a**–**s**.

*4.2.2.1. 12N-N′-p-Chlorophenylcarbamoylmethyl aloperine (**11a**).* Yield 48%; white solid; m.p. 169–171 °C. ^{1}H NMR (500 MHz, $CDCl_3$) δ 9.32 (s, 1H), 7.51–7.35 (m, 4H), 5.62 (d, J = 5.5 Hz, 1H), 3.67–3.49 (m, 1H), 2.95–2.87 (m, 2H), 2.79–2.71 (m, 1H), 2.68–2.61 (m, 2H), 2.58–2.50 (m, 1H), 2.47–2.41 (m, 1H), 2.34–2.24 (m, 2H), 2.12–2.13 (m, 1H), 2.08–1.97 (m, 2H), 1.93–1.85 (m, 2H), 1.80–1.73 (m, 1H), 1.73–1.66 (m, 1H), 1.63–1.50 (m, 2H), 1.50–1.41 (m, 2H), 1.40–1.35 (m, 1H), 1.34–1.23 (m, 2H); ^{13}C NMR (126 MHz) δ 169.6, 137.0, 132.9, 132.1 (2), 129.2, 120.8 (2), 116.6, 64.1, 63.7, 57.3, 55.8, 55.2, 51.5, 35.6, 33.3, 31.4, 30.2, 26.0, 25.4, 24.6, 23.7. ESI-HRMS: calcd for $C_{23}H_{31}ClN_3O$ $[M + H]^+$: 400.2150, found: 400.2152.

*4.2.2.2. 12N-N′-p-Bromophenylcarbamoylmethyl aloperine (**11b**).* Yield 47%; white solid; m.p. 168–170 °C. ^{1}H NMR (500 MHz, $CDCl_3$) δ 9.31 (s, 1H), 7.50 (d, J = 9.0 Hz, 2H), 7.30–7.25 (m, 2H), 5.62 (d, J = 5.5 Hz, 1H), 3.70–3.47 (m, 1H), 2.94–2.88 (m, 2H), 2.81–2.71 (m, 1H), 2.68–2.62 (m, 2H), 2.59–2.52 (m, 1H), 2.47–2.41 (m, 1H), 2.34–2.25 (m, 2H), 2.22–2.14 (m, 1H), 2.08–1.97 (m, 2H), 1.93–1.85 (m, 2H), 1.79–1.67 (m, 2H), 1.64–1.50 (m, 2H), 1.50–1.42 (m, 2H), 1.41–1.35 (m, 1H), 1.34–1.24 (m, 2H); ^{13}C NMR (126 MHz) δ 169.6, 136.6, 133.0, 129.3 (3), 129.1, 120.5 (2), 64.2, 63.8, 57.4, 55.9, 55.3, 51.6, 35.7, 33.4, 31.5, 30.3, 26.1, 25.5, 24.7, 23.8. ESI-HRMS: calcd for $C_{23}H_{31}BrN_3O$ $[M + H]^+$: 444.1645, found: 444.1646.

*4.2.2.3. 12N-N′-p-Iodophenylcarbamoylmethyl aloperine (**11c**).* Yield 35%; pink solid; m.p. 192–194 °C. ^{1}H NMR (400 MHz, DMSO-d_6) δ 11.21 (br, 1H), 7.79–7.37 (m, 4H), 5.78 (s, 1H), 4.57 (s, 1H), 4.44–4.10 (m, 1H), 3.73 (s, 1H), 3.60–3.31 (m, 5H), 3.30–3.08 (m, 3H), 2.78 (s, 1H), 2.45–2.23 (m, 3H), 2.21–2.03 (m, 2H), 1.85–1.53 (m, 6H), 1.45 (s, 1H); ^{13}C NMR (151 MHz) δ 162.6, 138.0, 137.3 (2), 134.1, 128.0, 121.7 (2), 88.1, 63.0, 58.1, 54.6, 53.8, 52.6, 45.1, 32.6, 30.1, 27.3, 22.8, 22.5, 22.0, 20.7, 17.7. ESI-HRMS: calcd for $C_{23}H_{31}IN_3O$ $[M + H]^+$, 492.1506, found: 492.1495.

*4.2.2.4. 12N-N′-(2,4-Dichlorophenyl)carbamoylmethyl aloperine (**11d**).* Yield 24%; brown solid; m.p. 71–73 °C. ^{1}H NMR (500 MHz, $CDCl_3$) δ 9.83 (s, 1H), 8.54–8.49 (m, 1H), 7.43–7.33 (m, 1H), 7.26–7.22 (m, 1H), 5.65 (s, 1H), 3.74–3.64 (m, 1H), 3.00–2.87 (m, 2H), 2.82–2.70 (m, 2H), 2.65 (s, 2H), 2.34–2.20 (m, 2H), 2.15–1.85 (m, 5H), 1.80–1.41 (m, 8H), 1.39–1.23 (m, 2H); ^{13}C NMR (126 MHz) δ 169.8, 133.7, 132.6, 129.5, 129.0, 128.9, 128.1, 123.1, 121.5, 65.5, 63.8, 57.6, 56.0, 55.1, 52.1, 35.6, 33.4, 32.4, 29.9, 25.8, 25.2 (2), 23.5. ESI-HRMS: calcd for $C_{23}H_{30}Cl_2N_3O$ $[M + H]^+$, 434.1760, found: 434.1766.

*4.2.2.5. 12N-N′-(2,5-Dibromophenyl)carbamoylmethyl aloperine (**11e**).* Yield 20%; light brown solid; m.p. 79–81 °C. ^{1}H NMR (500 MHz, $CDCl_3$) δ 9.81 (s, 1H), 8.78 (d, J = 2.5 Hz, 1H), 7.40–7.36 (m, 1H), 7.13–7.06 (m, 1H), 5.65 (s, 1H), 3.75–3.67 (m, 1H), 2.98–2.88 (m, 2H), 2.82–2.71 (m, 2H), 2.63 (s, 3H), 2.36–2.18 (m, 3H), 2.09–2.02 (m, 2H), 1.91 (s, 1H), 1.78–1.65 (m, 4H), 1.60–1.40 (m, 4H), 1.34–1.23 (m, 2H); ^{13}C NMR (101 MHz) δ 170.0, 137.2, 133.3, 132.3, 129.6, 127.8, 123.6, 122.2, 111.3, 65.2, 63.9, 57.7, 56.0, 55.1, 52.2, 35.7, 33.4, 32.6, 30.1, 25.7, 25.4, 25.3, 23.5. ESI-HRMS: calcd for $C_{23}H_{30}Br_2N_3O$ $[M + H]^+$, 522.0750, found: 522.0734.

*4.2.2.6. 12N-N′-(5-Bromo-2-fluorophenyl)carbamoylmethyl aloperine (**11f**).* Yield 11%; brown solid; m.p. 107–109 °C. ^{1}H NMR (500 MHz, $CDCl_3$) δ 9.53 (s, 1H), 8.65–8.57 (m, 1H), 7.21–7.09 (m, 1H), 7.00–6.92 (m, 1H), 5.66 (s, 1H), 3.74–3.63 (m, 1H), 3.39–3.10 (m, 1H), 2.97–2.86 (m, 2H), 2.77–2.47 (m, 3H), 2.40–2.19 (m, 3H), 2.12–1.91 (m, 4H), 1.85–1.64 (m, 4H), 1.59–1.25 (m, 6H); ^{13}C NMR (126 MHz) δ 169.4, 151.3, 132.6, 129.0, 127.5, 126.7, 123.7, 117.1, 116.1, 63.4, 57.2, 55.6 (2), 54.9, 51.4, 35.2, 33.1, 31.8, 29.5, 25.6, 24.9, 24.6, 23.2. ESI-HRMS: calcd for $C_{23}H_{30}BrFN_3O$ $[M + H]^+$, 462.1551, found: 462.1557.

*4.2.2.7. 12N-N′-(5-Bromo-2-chlorophenyl)carbamoylmethyl aloperine (**11g**).* Yield 14%; brown solid; m.p. 75–77 °C. ^{1}H NMR (500 MHz, $CDCl_3$) δ 9.87 (s, 1H), 8.78 (d, J = 2.0 Hz, 1H), 7.25–7.21 (m, 1H), 7.19–7.14 (m, 1H), 5.65 (s, 1H), 3.76–3.69 (m, 1H), 2.97–2.88 (m, 2H), 2.82–2.74 (m, 1H), 2.63 (s, 3H), 2.35–2.22 (m, 2H), 2.11–2.01 (m, 3H), 1.92 (s, 1H), 1.78 (s, 2H), 1.71–1.60 (m, 3H), 1.58–1.41 (m, 4H),

1.36–1.25 (m, 2H); ^{13}C NMR (126 MHz) δ 169.6, 135.6, 132.1, 129.9, 129.3, 127.0, 123.1, 121.2, 121.0, 65.1, 63.4, 57.3, 55.6, 54.7, 51.8, 35.3, 33.1, 32.1, 29.6 (2), 25.5, 24.9, 23.2. ESI-HRMS: calcd for $C_{23}H_{30}BrClN_3O$ $[M + H]^+$, 478.1255, found: 478.1237.

*4.2.2.8. 12N-N′-(2-Fluoro-6-methylphenyl)carbamoylmethyl aloperine (**11h**).* Yield 15%; brown solid; m.p. 107–109 °C. ^{1}H NMR (500 MHz, $CDCl_3$) δ 9.92 (s, 1H), 7.14 (s, 1H), 7.06–6.87 (m, 2H), 5.67 (s, 1H), 3.80–3.64 (m, 1H), 3.58–3.35 (m, 3H), 3.30 (s, 1H), 3.19–3.05 (m, 1H), 2.98–2.67 (m, 3H), 2.64–2.46 (m, 2H), 2.38–2.23 (m, 5H), 2.17–1.91 (m, 4H), 1.85–1.72 (m, 3H), 1.65–1.48 (m, 3H), 1.32 (s, 1H); ^{13}C NMR (126 MHz) δ 170.2, 158.9, 141.2, 138.2, 129.1, 128.0, 126.1, 123.3, 113.3, 61.9, 56.3, 55.9, 55.2, 51.7, 45.7, 35.6, 33.5, 32.2, 29.8, 25.7, 25.1, 24.0, 23.4, 18.6. ESI-HRMS: calcd for $C_{24}H_{33}FN_3O$ $[M + H]^+$, 398.2602, found: 398.2602.

*4.2.2.9. 12N-N′-(2-Chloro-4-methylphenyl)carbamoylmethyl aloperine (**11i**).* Yield 25%; brown solid; m.p. 72–74 °C. ^{1}H NMR (500 MHz, $CDCl_3$) δ 9.73 (s, 1H), 8.44–8.33 (m, 1H), 7.21–7.15 (m, 1H), 7.12–7.04 (m, 1H), 5.69–5.60 (m, 1H), 3.75–3.66 (m, 1H), 3.03–2.85 (m, 2H), 2.64 (s, 4H), 2.35–2.21 (m, 5H), 2.12–1.99 (m, 3H), 1.91 (s, 1H), 1.81–1.60 (m, 5H), 1.56–1.38 (m, 4H), 1.35–1.23 (m, 2H); ^{13}C NMR (126 MHz) δ 169.6, 134.5, 132.6, 132.4 129.5, 129.5, 128.5, 122.5, 120.7, 65.4, 63.8, 57.6, 55.9, 55.0, 52.1, 35.7, 33.5, 32.6, 30.0, 25.8, 25.4, 25.3, 23.5, 20.9. ESI-HRMS: calcd for $C_{24}H_{33}ClN_3O$ $[M + H]^+$, 414.2307, found: 414.2309.

*4.2.2.10. 12N-N′-(4-Chloro-2-methylphenyl)carbamoylmethyl aloperine (**11j**).* Yield 23%; brown solid; m.p. 90–92 °C. ^{1}H NMR (500 MHz, $CDCl_3$) δ 9.21 (s, 1H), 8.25–8.15 (m, 1H), 7.22–7.10 (m, 2H), 5.64 (s, 1H), 3.77–3.63 (m, 1H), 2.99–2.87 (m, 2H), 2.82–2.59 (m, 4H), 2.48 (s, 1H), 2.33–2.21 (m, 5H), 2.12–2.01 (m, 3H), 1.92 (s, 1H), 1.81–1.68 (m, 3H), 1.62–1.39 (m, 5H), 1.34–1.23 (m, 2H); ^{13}C NMR (126 MHz) δ 169.3, 134.9, 132.7, 130.3, 129.5, 129.0, 128.3, 127.1, 121.7, 64.9, 63.8, 57.5, 56.0, 55.1, 52.0, 35.7, 33.4, 32.0, 30.1, 26.1, 25.3, 25.0, 23.6, 18.1. ESI-HRMS: calcd for $C_{24}H_{33}ClN_3O$ $[M + H]^+$, 414.2307, found: 414.2310.

*4.2.2.11. 12N-N′-(3-Chloro-5-trifluoromethylphenyl)carbamoylmethyl aloperine (**11k**).* Yield 53%; brown solid; m.p. 74–76 °C. ^{1}H NMR (500 MHz, $CDCl_3$) δ 9.58 (s, 1H), 7.90 (s, 1H), 7.65 (s, 1H), 7.33 (s, 1H), 5.66 (s, 1H), 3.71–3.48 (m, 1H), 3.00–2.86 (m, 2H), 2.83–2.74 (m, 1H), 2.71–2.40 (m, 4H), 2.39–2.19 (m, 3H), 2.13–1.92 (m, 4H), 1.81–1.30 (m, 9H); ^{13}C NMR (126 MHz) δ 170.0, 139.7, 135.5, 132.8, 129.1, 124.3, 122.2, 120.9, 114.1, 63.6, 57.2, 55.7, 55.4, 51.2, 35.5, 33.3, 30.8, 30.2, 29.8, 25.9, 25.3, 24.2, 23.7 (2). ESI-HRMS: calcd for $C_{24}H_{30}ClF_3N_3O$ $[M + H]^+$, 468.2024, found: 468.2027.

*4.2.2.12. 12N-N′-(4-Bromo-3-trifluoromethylphenyl)carbamoylmethyl aloperine (**11m**)..* Yield 34%; brown solid; m.p. 70–71 °C. ^{1}H NMR (500 MHz, $CDCl_3$) δ 9.52 (s, 1H), 7.83 (d, J = 2.0 Hz, 1H), 7.74–7.70 (m, 1H), 7.64 (s, 1H), 5.65 (d, J = 5.0 Hz, 1H), 3.64–3.59 (m, 1H), 2.97–2.89 (m, 2H), 2.83–2.76 (m, 1H), 2.71–2.61 (m, 2H), 2.56–2.51 (m, 1H), 2.47–2.42 (m, 1H), 2.37–2.29 (m, 2H), 2.25–2.18 (m, 1H), 2.09–1.99 (m, 2H), 1.97–1.89 (m, 2H), 1.79–1.70 (m, 2H), 1.66–1.43 (m, 4H), 1.41–1.27 (m, 3H); ^{13}C NMR (126 MHz) δ 169.7, 137.1, 135.4, 132.8, 128.9, 123.1, 121.4, 118.2, 113.4, 63.5, 63.4, 57.0, 55.5, 55.1, 51.1, 35.4, 33.0, 30.7, 30.1, 29.6, 25.7, 25.1, 24.0, 23.6. ESI-HRMS: calcd for $C_{24}H_{30}BrF_3N_3O$ $[M + H]^+$, 512.1519, found: 512.1524.

*4.2.2.13. 12N-N′-(3,4-Dimethylphenyl)carbamoylmethyl aloperine (**11n**).* Yield 46%; white solid; m.p. 58–60 °C. ^{1}H NMR (400 MHz, DMSO-d_6) δ 9.40 (s, 1H), 7.39–7.23 (m, 2H), 7.05 (d, J = 7.6 Hz, 1H), 5.54 (s, 1H), 3.50–3.41 (m, 1H), 3.32 (s, 2H), 3.00–2.91 (m, 1H), 2.91–2.79 (m, 2H), 2.57 (s, 3H), 2.45–2.34 (m, 2H), 2.21–2.11 (m, 7H), 2.00–1.86 (m, 2H), 1.85–1.73 (m, 2H), 1.72–1.64 (m, 1H), 1.63–1.54 (m, 1H), 1.51–1.29 (m, 5H), 1.19–1.10 (m, 1H); ^{13}C NMR (101 MHz, $CDCl_3$) δ 169.2, 137.4, 135.7, 133.2, 132.5, 130.1, 129.0, 120.7, 116.9, 64.2, 63.8, 57.3, 55.7, 55.1, 51.4, 35.7, 33.4, 31.4, 30.2, 26.0, 25.4, 24.6, 23.7, 20.0, 19.3. ESI-HRMS: calcd for $C_{25}H_{36}N_3O$ $[M + H]^+$, 394.2853, found: 394.2840.

*4.2.2.14. 12N-N′-(3,5-Ditrifluoromethylphenyl)carbamoylmethyl aloperine (**11o**).* Yield 36%; white solid; m.p. 94–96 °C. ^{1}H NMR (400 MHz, DMSO-d_6) δ 10.24 (s, 1H), 8.34 (s, 2H), 7.76 (s, 1H), 5.53 (d, J = 5.2 Hz, 1H), 3.58–3.48 (m, 1H), 3.41–3.30 (m, 1H), 3.19–3.08 (m, 1H), 2.99 (s, 1H), 2.94–2.84 (m, 1H), 2.62–2.53 (m, 3H), 2.49–2.40 (m, 1H), 2.25–2.16 (m, 1H), 2.08–1.87 (m, 3H), 1.81 (s, 1H), 1.75–1.64 (m, 2H), 1.57 (s, 2H), 1.47–1.34 (m, 3H), 1.33–1.20 (m, 2H), 1.17–1.08 (m, 1H); ^{13}C NMR (101 MHz, $CDCl_3$) δ 170.3, 139.4, 133.2, 132.5 (2), 129.1, 123.3 (2), 119.0, 117.4 (2), 63.8, 63.4, 57.3, 55.6, 55.5, 51.2, 35.6, 33.3, 30.6, 30.4, 25.9, 25.4, 24.0, 23.9. ESI-HRMS: calcd for $C_{25}H_{30}F_6N_3O$ $[M + H]^+$: 502.2288, found: 502.2277.

*4.2.2.15. 12N-N′-(2-Naphthyl)carbamoylmethyl aloperine (**11p**).* Yield 39%; white solid; m.p. 64–66 °C. ^{1}H NMR (400 MHz, $CDCl_3$) δ 9.46 (s, 1H), 8.24 (s, 1H), 7.79 (t, J = 9.2 Hz, 3H), 7.52–7.42 (m, 2H), 7.39 (t, J = 7.6 Hz, 1H), 5.65 (d, J = 4.8 Hz, 1H), 3.74–3.63 (m, 1H), 3.04–2.91 (m, 2H), 2.87–2.77 (m, 1H), 2.76–2.64 (m, 2H), 2.60 (s, 1H), 2.38–2.28 (m, 2H), 2.27–2.18 (m, 1H), 2.13–1.98 (m, 2H), 1.97–1.89 (d, J = 8.0 Hz, 2H), 1.80–1.62 (m, 3H), 1.59–1.28 (m, 6H), 1.24 (t, J = 6.8 Hz, 1H); ^{13}C NMR (101 MHz) δ 169.7, 135.4, 134.0, 133.1, 130.7, 129.1, 129.0, 127.7, 127.7, 126.6, 125.0, 119.5, 115.9, 64.1, 63.9, 57.4, 55.8, 55.3, 51.5, 35.7, 33.4, 31.4, 30.3, 26.1, 25.4, 24.6, 23.8. ESI-HRMS: calcd for $C_{27}H_{34}N_3O$ $[M + H]^+$: 416.2696, found: 416.2696.

*4.2.2.16. 12N-N′-(2-Quinolyl)carbamoylmethyl aloperine (**11q**).* Yield 32%; white solid; m.p. 78–80 °C. ^{1}H NMR (400 MHz, $CDCl_3$) δ 9.77 (s, 1H), 8.43 (d, J = 8.8 Hz, 1H), 8.15 (d, J = 8.8 Hz, 1H), 7.85 (d, J = 8.4 Hz, 1H), 7.76 (d, J = 8.0 Hz, 1H), 7.64 (t, J = 7.2 Hz, 1H), 7.43 (t, J = 7.2 Hz, 1H), 5.66 (s, 1H), 3.76–3.62 (m, 1H), 3.07–2.98 (m, 1H), 2.94 (s, 1H), 2.88–2.80 (m, 1H), 2.79–2.52 (m, 4H), 2.41–2.22 (m, 3H), 2.14–1.90 (m, 4H), 1.88–1.75 (m, 2H), 1.73–1.66 (m, 1H), 1.60–1.19 (m, 6H); ^{13}C NMR (101 MHz) δ 170.8, 150.6, 147.0, 138.4, 133.3, 129.9, 128.9, 127.9, 127.6, 126.5, 125.2, 114.3, 64.2, 58.0 (2), 55.6, 55.4, 51.2, 35.7, 33.4, 31.5, 30.2, 25.7, 25.4, 24.6, 23.8. ESI-HRMS: calcd for $C_{26}H_{33}N_4O$ $[M + H]^+$, 417.2649, found: 417.2638.

*4.2.2.17. 12N-N′-p-Bromophenyl-N′-methylcarbamoylmethyl aloperine hydrochloride (**11r**).* Yield 45%; white solid; m.p. 157–159 °C. ^{1}H NMR (400 MHz, $CDCl_3$) δ 10.80 (s, 1H), 7.60 (d, J = 7.2 Hz, 2H), 7.13 (d, J = 8.4 Hz, 2H), 5.61 (s, 1H), 3.37 (d, J = 5.6 Hz, 1H), 3.27–3.18 (m, 4H), 2.99–2.79 (m, 4H), 2.77–2.68 (m, 1H), 2.67–2.48 (m, 4H), 2.25–2.16 (m, 1H), 2.16–2.06 (m, 2H), 1.98–1.90 (m, 2H), 1.84–1.70 (m, 3H), 1.68–1.60 (m, 1H), 1.56–1.38 (m, 3H), 1.24 (s, 1H); ^{13}C NMR (101 MHz) δ 169.4, 142.2, 135.4, 133.5 (2), 129.3 (2), 125.8, 122.2, 68.9, 62.5, 55.9, 54. 9, 53.0, 50.7, 37.5, 33.7, 32.9, 30.6, 27.3, 25.6, 23.5, 22.8, 22.5. ESI-HRMS: calcd for $C_{24}H_{33}BrN_3O$ •HCl [M-HCl + H]$^+$, 458.1802, found: 458.1790.

*4.2.3. General procedure for 12N-substituted aminoacetyl aloperines (**14a–r**)*

To a mixture of the different substituted amines **12a–r** (5 mmol) and $NaHCO_3$ (0.5 g, 6 mmol) in anhydrous ethanol (50 mL), ethyl bromoacetate (1.1 g, 5.5 mmol) was added. The mixture was refluxed for 8 h, and then poured into water (30 mL) and extracted with ethyl acetate (50 mL). The organic layer was concentrated to give crude products, which was directly added to a solution of LiOH (5.5 mmol) in H_2O (40 mL), and the mixture was refluxed for 1.5 h. After cooling, the pH of the mixture was acidified to 2 by 3 N HCl and extracted with CH_2Cl_2 (20 mL × 2). , the organic layer was concentrated to give crude products **13a–r** for the next step directly.

To a solution of **13a–r** (2 mmol) in anhydrous CH_2Cl_2 (30 mL) at

0 °C, *N*-hydroxy benzotrizol (HOBt, 2.7 mmol), diisopropylethylamine (5.2 mL) and 1-ethyl-3-(3-dimethylaminopropyl) carbodiimide (EDCI, 4 mmol) were added. The mixture was stirred for 30 min before the addition of aloperine (2.1 mmol), and was warmed to r.t. and stirred for 12 h. The mixture was washed with water and brine (30 mL), dried over anhydrous Na_2SO_4, filtered and then the filtrate was concentrated in vacuo. The residue was purified by flash column chromatography on silica gel with CH_2Cl_2/CH_3OH as the eluent to give the products **14a**–**r**.

*4.2.3.1. 12N-N′-Phenylaminoacetyl aloperine (**14a**).* Yield 58%; white solid; m.p. 62–64 °C. ^{1}H NMR (400 MHz, $CDCl_3$) δ 7.19 (t, J = 7.6 Hz, 2H), 6.72 (t, J = 7.2 Hz, 1H), 6.64 (d, J = 8.0 Hz, 2H), 5.65 (s, 1H), 4.95 (s, 1H), 4.76 (s, 1H), 4.06–3.90 (m, 1H), 3.91–3.80 (m, 1H), 3.79–3.65 (m, 1H), 3.49–3.38 (m, 1H), 3.12–2.98 (m, 1H), 2.75 (d, J = 6.8 Hz, 2H), 2.65–2.54 (m, 1H), 2.45 (s, 1H), 2.40–2.32 (m, 1H), 2.31–2.21 (m, 1H), 2.17–2.06 (m, 1H), 1.97 (s, 1H), 1.92–1.76 (m, 5H), 1.73–1.62 (m, 2H), 1.51–1.39 (m, 1H), 1.16–1.01 (m, 2H); ^{13}C NMR (101 MHz) δ 167.9, 147.6, 135.5, 129.4 (2), 128. 4, 117.5, 113.1 (2), 59.4, 59.2, 54.4, 46.9, 45.5, 40.6, 35.1, 31.5, 28.0, 26.3, 24.9, 24.7, 24.1, 19.2. ESI-HRMS: calcd for $C_{23}H_{32}N_3O$ [M + H]$^+$: 366.2540, found: 366.2540.

*4.2.3.2. 12N-N′-p-Fluorophenylaminoacetyl aloperine (**14b**).* Yield 42%; white solid; m.p. 64–66 °C. ^{1}H NMR (600 MHz, $CDCl_3$) δ 6.92–6.86 (m, 2H), 6.59–6.53 (m, 2H), 5.64 (d, J = 4.2 Hz, 1H), 4.82 (s, 1H), 4.75 (d, J = 4.8 Hz, 1H), 3.97–3.89 (m, 1H), 3.84–3.77 (m, 1H), 3.77–3.67 (m, 1H), 3.47–3.30 (m, 1H), 3.11–3.01 (m, 1H), 2.79–2.70 (m, 2H), 2.63–2.54 (m, 1H), 2.44 (s, 1H), 2.39–2.32 (m, 1H), 2.30–2.21 (m, 1H), 2.16–2.07 (m, 1H), 2.05–1.95 (m, 1H), 1.94–1.73 (m, 5H), 1.72–1.60 (m, 2H), 1.49–1.39 (m, 1H), 1.15–1.02 (m, 2H); ^{13}C NMR (151 MHz) δ 167.9, 156.0, 144.2, 135.4, 128.5, 115.9, 115.7, 113.9, 113.8, 59.5, 59.3, 54.5, 46.9, 46.2, 40.6, 35.2, 31.6, 28.1, 26.3, 24.9, 24.7, 24.2, 19.3. ESI-HRMS: calcd for $C_{23}H_{31}FN_3O$ [M + H]$^+$: 384.2446, found: 384.2447.

*4.2.3.3. 12N-N′-m-Fluorophenylaminoacetyl aloperine (**14c**).* Yield 40%; white solid; m.p. 64–66 °C. ^{1}H NMR (600 MHz, $CDCl_3$) δ 7.13–7.06 (m, 1H), 6.43–6.35 (m, 2H), 6.31–6.24 (m, 1H), 5.65 (d, J = 5.4 Hz, 1H), 5.10 (s, 1H), 4.75 (d, J = 4.8 Hz, 1H), 3.99–3.90 (m, 1H), 3.84–3.78 (m, 1H), 3.78–3.71 (m, 1H), 3.46–3.32 (m, 1H), 3.12–3.01 (m, 1H), 2.79–2.70 (m, 2H), 2.64–2.56 (m, 1H), 2.45 (s, 1H), 2.38–2.32 (m, 1H), 2.31–2.22 (m, 1H), 2.20–2.07 (m, 1H), 2.00–1.95 (m, 1H), 1.95–1.81 (m, 4H), 1.81–1.73 (m, 1H), 1.72–1.62 (m, 2H), 1.50–1.38 (m, 1H), 1.15–1.03 (m, 2H); ^{13}C NMR (151 MHz) δ 167.4, 164.3, 149.4, 135.3, 130.4, 128.6, 109.1, 103.9, 99.6, 59.5, 59.4, 54.5, 46.9, 45.4, 40.6, 35.2, 31.6, 28.1, 26.3, 24.9, 24.7, 24.1, 19.3. ESI-HRMS: calcd for $C_{23}H_{31}FN_3O$ [M + H]$^+$: 384.2446, found: 384.2449.

*4.2.3.4. 12N-N′-p-Chlorophenylaminoacetyl aloperine (**14d**).* Yield 45%; white solid; m.p. 73–75 °C. ^{1}H NMR (400 MHz, $CDCl_3$) δ 7.12 (d, J = 8.8 Hz, 2H), 6.54 (d, J = 8.4 Hz, 2H), 5.64 (d, J = 4.0 Hz, 1H), 4.99 (s, 1H), 4.74 (d, J = 4.4 Hz, 1H), 4.02–3.86 (m, 1H), 3.84–3.65 (m, 2H), 3.46–3.31 (m, 1H), 3.12–2.98 (m, 1H), 2.74 (d, J = 7.6 Hz, 2H), 2.65–2.54 (m, 1H), 2.43 (s, 1H), 2.38–2.21 (m, 2H), 2.18–2.04 (m, 1H), 1.97 (s, 1H), 1.93–1.74 (m, 5H), 1.72–1.61 (m, 2H), 1.51–1.35 (m, 1H), 1.15–0.99 (m, 2H); ^{13}C NMR (101 MHz) δ 167.5, 146.1, 135.3, 129.2 (2), 128.5, 122.0, 114.1 (2), 59.4, 59.3, 54.4, 46.9, 45.5, 40.6, 35.1, 31.5, 28.0, 26.3, 24.9, 24.6, 24.0, 19.2. ESI-HRMS: calcd for $C_{23}H_{31}ClN_3O$ [M + H]$^+$: 400.2150, found: 400.2152.

*4.2.3.5. 12N-N′-p-Bromophenylaminoacetyl aloperine (**14e**).* Yield 43%; white solid; m.p. 73–75 °C. ^{1}H NMR (600 MHz, DMSO-d_6) δ 7.22–7.17 (m, 2H), 6.63 (d, J = 8.4 Hz, 2H), 5.79 (t, J = 4.8 Hz, 1H), 5.60 (d, J = 5.4 Hz, 1H), 4.54 (d, J = 5.4 Hz, 1H), 4.00–3.94 (m, 1H), 3.88–3.80 (m, 1H), 3.67–3.60 (m, 1H), 3.52–3.45 (m, 1H), 2.98–2.90 (m, 1H), 2.76–2.70 (m, 1H), 2.68–2.62 (m, 1H), 2.55–2.51 (m, 1H), 2.35–2.30 (m, 1H), 2.26 (s, 1H), 2.23–2.14 (m, 1H), 2.05–1.86 (m, 3H), 1.84–1.74 (m, 3H), 1.67–1.51 (m, 3H), 1.45–1.34 (m, 1H), 1.09–0.98 (m, 2H); ^{13}C NMR (151 MHz, $CDCl_3$) δ 167.5, 146.6, 135.3, 132.1 (2), 128.6, 114.6 (2), 109.1, 59.5, 59.4, 54.5, 46.9, 45.4, 40.6, 35.2, 31.6, 28.1, 26.3, 24.9, 24.7, 24.1, 19.3. ESI-HRMS: calcd for $C_{23}H_{31}BrN_3O$ [M + H]$^+$: 444.1645, found: 444.1651.

*4.2.3.6. 12N-N′-p-Iodophenylaminoacetyl aloperine (**14f**).* Yield 46%; white solid; m.p. 85–87 °C. ^{1}H NMR (600 MHz, $CDCl_3$) δ 7.42 (d, J = 8.4 Hz, 2H), 6.41 (d, J = 8.4 Hz, 2H), 5.64 (d, J = 5.4 Hz, 1H), 5.07–4.97 (m, 1H), 4.74 (d, J = 6.6 Hz, 1H), 3.94–3.88 (m, 1H), 3.82–3.70 (m, 2H), 3.44–3.36 (m, 1H), 3.07–3.02 (m, 1H), 2.78–2.71 (m, 2H), 2.62–2.56 (m, 1H), 2.44 (s, 1H), 2.37–2.31 (m, 1H), 2.29–2.22 (m, 1H), 2.19–2.07 (m, 1H), 2.00–1.95 (m, 1H), 1.94–1.73 (m, 5H), 1.72–1.62 (m, 2H), 1.49–1.38 (m, 1H), 1.15–1.03 (m, 2H); ^{13}C NMR (151 MHz) δ 167.4, 147.2, 137.9 (3), 135.3, 128.6, 115.3 (2), 59.5, 59.4, 54.5, 46.9, 45.3, 40.6, 35.2, 31.6, 28.1, 26.3, 24.9, 24.7, 24.1, 19.3. ESI-HRMS: calcd for $C_{23}H_{31}IN_3O$ [M + H]$^+$: 492.1506, found: 492.1517.

*4.2.3.7. 12N-N′-p-Tolylaminoacetyl aloperine (**14g**).*. Yield 48%; white solid; m.p. 59–61 °C. ^{1}H NMR (400 MHz, $CDCl_3$) δ 7.00 (d, J = 8.0 Hz, 2H), 6.56 (d, J = 8.4 Hz, 2H), 5.68–5.59 (m, 1H), 4.83–4.72 (m, 2H), 4.00–3.91 (m, 1H), 3.87–3.78 (m, 1H), 3.77–3.67 (m, 1H), 3.46–3.39 (m, 1H), 3.08–2.99 (m, 1H), 2.77–2.70 (m, 2H), 2.62–2.55 (m, 1H), 2.44 (s, 1H), 2.38–2.32 (m, 1H), 2.27–2.22 (m, 4H), 2.17–2.06 (m, 1H), 1.97 (s, 1H), 1.91–1.83 (m, 3H), 1.82–1.77 (m, 1H), 1.72–1.63 (m, 2H), 1.60 (s, 1H), 1.50–1.39 (m, 1H), 1.15–1.02 (m, 2H); ^{13}C NMR (101 MHz) δ 168.1, 145.5, 135.5, 129.8 (2), 128.4, 126.7, 113.2 (2), 59.4, 59.2, 54.4, 46.9, 45.9, 40.6, 35.1, 31.5, 28.0, 26.3, 24.9, 24.7, 24.1, 20.5, 19.2. ESI-HRMS: calcd for $C_{24}H_{34}N_3O$ [M + H]$^+$: 380.2696, found: 380.2685.

*4.2.3.8. 12N-N′-m-Trifluoromethylphenylaminoacetyl aloperine (**14h**).*. Yield 45%; white solid; m.p. 58–60 °C. ^{1}H NMR (600 MHz, DMSO-d_6) δ 7.26 (d, J = 8.4 Hz, 1H), 6.98–6.87 (m, 2H), 6.83 (d, J = 7.8 Hz, 1H), 6.14 (t, J = 4.8 Hz, 1H), 5.60 (d, J = 5.4 Hz, 1H), 4.60–4.51 (m, 1H), 4.10–4.02 (m, 1H), 3.96–3.88 (m, 1H), 3.71–3.64 (m, 1H), 3.54–3.46 (m, 1H), 2.97–2.89 (m, 1H), 2.75–2.69 (m, 1H), 2.69–2.62 (m, 1H), 2.56–2.51 (m, 1H), 2.36–2.29 (m, 1H), 2.28–2.16 (m, 2H), 2.04–1.96 (m, 1H), 1.95–1.88 (m, 2H), 1.84–1.74 (m, 3H), 1.68–1.58 (m, 2H), 1.58–1.50 (m, 1H), 1.45–1.33 (m, 1H), 1.09–0.97 (m, 2H); ^{13}C NMR (101 MHz, $CDCl_3$) δ 167.2, 147.7, 135.3, 131.7, 129.7, 128.6, 124.5, 116.6, 113.8, 108.5, 59.4 (2), 54.4, 46.9, 45.1, 40.6, 35.1, 31.5, 28.0, 26.3, 24.9, 24.7, 24.1, 19.2. ESI-HRMS: calcd for $C_{24}H_{31}F_3N_3O$ [M + H]$^+$: 434.2414, found: 434.2403.

*4.2.3.9. 12N-N′-m-Methoxyphenylaminoacetyl aloperine (**14i**).* Yield 50%; white solid; m.p. 60–62 °C. ^{1}H NMR (400 MHz, $CDCl_3$) δ 7.09 (t, J = 8.0 Hz, 1H), 6.27 (td, J = 8.0, 2.0 Hz, 2H), 6.17 (t, J = 2.0 Hz, 1H), 5.67–5.59 (m, 1H), 5.01–4.93 (m, 1H), 4.75 (d, J = 5.6 Hz, 1H), 3.99–3.91 (m, 1H), 3.86–3.79 (m, 1H), 3.78 (s, 3H), 3.76–3.68 (m, 1H), 3.45–3.37 (m, 1H), 3.08–3.01 (m, 1H), 2.77–2.71 (m, 2H), 2.62–2.56 (m, 1H), 2.47–2.40 (m, 1H), 2.39–2.32 (m, 1H), 2.31–2.22 (m, 1H), 2.16–2.06 (m, 1H), 2.00–1.94 (m, 1H), 1.93–1.83 (m, 3H), 1.82–1.65 (m, 3H), 1.65–1.60 (m, 1H), 1.50–1.40 (m, 1H), 1.14–1.02 (m, 2H); ^{13}C NMR (101 MHz) δ 167.7, 160.9, 149.0, 135.4, 130.1, 128.5, 106.3, 102.5, 99.1, 59.4, 59.2, 55.2, 54.4, 46.9, 45.5, 40.6, 35.1, 31.5, 28.0, 26.3, 24.9, 24.6, 24.1, 19.2. ESI-HRMS: calcd for $C_{24}H_{34}N_3O_2$ [M + H]$^+$: 396.2646, found: 396.2634.

*4.2.3.10. 12N-N′-p-Trifluoromethoxyphenylaminoacetyl aloperine (**14j**).* Yield 35%; white solid; m.p. 57–59 °C. ^{1}H NMR (600 MHz, $CDCl_3$) δ 7.04 (d, J = 8.4 Hz, 2H), 6.61–6.54 (m, 2H), 5.65 (d, J = 4.2 Hz, 1H), 5.03 (s, 1H), 4.75 (d, J = 4.2 Hz, 1H), 4.00–3.91 (m, 1H), 3.85–3.79 (m, 1H), 3.78–3.66 (m, 1H), 3.45–3.33 (m, 1H), 3.13–3.00 (m, 1H), 2.74 (d, J = 7.8 Hz, 2H), 2.64–2.56 (m, 1H), 2.44 (s, 1H), 2.38–2.31 (m, 1H),

2.31–2.22 (m, 1H), 2.18–2.08 (m, 1H), 2.00–1.95 (m, 1H), 1.95–1.81 (m, 4H), 1.81–1.73 (m, 1H), 1.72–1.62 (m, 2H), 1.49–1.39 (m, 1H), 1.15–1.02 (m, 2H); ^{13}C NMR (151 MHz) δ 167.5, 146.5, 140.7, 135.3, 128.6, 122.5 (2), 120.9, 113.3 (2), 59.5, 59.4, 54.5, 47.0, 45.7, 40.7, 35.2, 31.6, 28.1, 26.3, 24.9, 24.7, 24.1, 19.3. ESI-HRMS: calcd for $C_{24}H_{31}F_3N_3O_2$ $[M + H]^+$: 450.2363, found: 450.2363.

*4.2.3.11. 12N-N′-(2,4-Dichlorophenylamino)acetyl aloperine (**14k**)..* Yield 46%; white solid; m.p. 79–81 °C. ^{1}H NMR (600 MHz, $CDCl_3$) δ 7.27 (d, J = 2.4 Hz, 1H), 7.09 (dd, J = 8.4, 2.4 Hz, 1H), 6.46 (d, J = 8.4 Hz, 1H), 5.71–5.62 (m, 2H), 4.77 (d, J = 5.4 Hz, 1H), 4.02–3.92 (m, 1H), 3.88–3.81 (m, 1H), 3.80–3.69 (m, 1H), 3.44–3.34 (m, 1H), 3.11–3.00 (m, 1H), 2.78–2.70 (m, 2H), 2.62–2.56 (m, 1H), 2.47 (s, 1H), 2.39–2.32 (m, 1H), 2.31–2.20 (m, 1H), 2.19–2.08 (m, 1H), 1.97 (s, 1H), 1.92–1.75 (m, 5H), 1.72–1.62 (m, 2H), 1.49–1.38 (m, 1H), 1.15–1.02 (m, 2H); ^{13}C NMR (151 MHz) δ 167.0, 142.3, 135.2, 129.1, 128.6, 127.7, 121.4, 120.2, 111.8, 59.5 (2), 54.5, 47.0, 45.3, 40.7, 35.2, 31.6, 28.0, 26.3, 24.9, 24.7, 24.1, 19.3. ESI-HRMS: calcd for $C_{23}H_{30}Cl_2N_3O$ $[M + H]^+$: 434.1760, found: 434.1772.

*4.2.3.12. 12N-N′-(3,4-Dichlorophenylamino)acetyl aloperine (**14l**)..* Yield 43%; white solid; m.p. 67–69 °C. ^{1}H NMR (600 MHz, $CDCl_3$) δ 7.20–7.16 (m, 1H), 6.64 (d, J = 3.0 Hz, 1H), 6.47 (dd, J = 9.0, 3.0 Hz, 1H), 5.65 (d, J = 4.8 Hz, 1H), 5.13–5.05 (m, 1H), 4.74 (d, J = 5.4 Hz, 1H), 3.95–3.87 (m, 1H), 3.81–3.72 (m, 2H), 3.43–3.35 (m, 1H), 3.08–3.02 (m, 1H), 2.78–2.70 (m, 2H), 2.64–2.56 (m, 1H), 2.43 (s, 1H), 2.37–2.32 (m, 1H), 2.31–2.24 (m, 1H), 2.19–2.07 (m, 1H), 2.05–1.95 (m, 1H), 1.95–1.81 (m, 4H), 1.81–1.74 (m, 1H), 1.71–1.60 (m, 2H), 1.49–1.38 (m, 1H), 1.15–1.02 (m, 2H); ^{13}C NMR (151 MHz) δ 167.1, 147.0, 135.2, 133.0, 130.8, 128.7, 119.9, 113.7, 113.2, 59.5, 59.4, 54.4, 46.9, 45.2, 40.7, 35.2, 31.6, 28.0, 26.3, 24.9, 24.7, 24.1, 19.3. ESI-HRMS: calcd for $C_{23}H_{30}Cl_2N_3O$ $[M + H]^+$: 434.1760, found: 434.1767.

*4.2.3.13. 12N-N′-(3,5-Dimethylphenylamino)acetyl aloperine (**14m**)..* Yield 54%; white solid; m.p. 64–66 °C. ^{1}H NMR (400 MHz, $CDCl_3$) δ 6.38 (s, 1H), 6.27 (s, 2H), 5.64 (d, J = 4.8 Hz, 1H), 4.84 (s, 1H), 4.75 (d, J = 4.8 Hz, 1H), 4.00–3.91 (m, 1H), 3.87–3.79 (m, 1H), 3.78–3.67 (m, 1H), 3.49–3.40 (m, 1H), 3.09–3.00 (m, 1H), 2.74 (d, J = 7.6 Hz, 2H), 2.63–2.54 (m, 1H), 2.44 (s, 1H), 2.38–2.31 (m, 1H), 2.25 (s, 7H), 2.16–2.06 (m, 1H), 1.97 (s, 1H), 1.92–1.83 (m, 3H), 1.82–1.74 (m, 2H), 1.72–1.62 (m, 2H), 1.47–1.39 (m, 1H), 1.15–1.02 (m, 2H); ^{13}C NMR (101 MHz) δ 168.0, 147.8, 139.0 (2), 135.5, 128.4, 119.5, 111.1 (2), 59.4, 59.2, 54.4, 46.8, 45.7, 40.6, 35.1, 31.5, 28.0, 26.3, 24.9, 24.7, 24.1, 21.6 (2), 19.2. ESI-HRMS: calcd for $C_{25}H_{36}N_3O$ $[M + H]^+$: 394.2853, found: 394.2841.**

*4.2.3.14. 12N-N′-(3,5-Dimethoxyphenylamino)acetyl aloperine (**14n**)..* Yield 39%; white solid; m.p. 61–63 °C. ^{1}H NMR (400 MHz, $CDCl_3$) δ 5.89 (s, 1H), 5.81 (s, 2H), 5.64 (d, J = 4.0 Hz, 1H), 4.98 (s, 1H), 4.74 (d, J = 4.8 Hz, 1H), 4.00–3.90 (m, 1H), 3.83 (d, J = 3.6 Hz, 1H), 3.76 (s, 6H), 3.45–3.34 (m, 1H), 3.11–2.99 (m, 1H), 2.74 (d, J = 8.0 Hz, 2H), 2.63–2.54 (m, 1H), 2.43 (s, 1H), 2.38–2.31 (m, 1H), 2.30–2.20 (m, 1H), 2.17–2.05 (m, 1H), 1.97 (s, 1H), 1.94–1.74 (m, 5H), 1.73–1.62 (m, 3H), 1.50–1.38 (m, 1H), 1.15–1.01 (m, 2H); ^{13}C NMR (101 MHz) δ 167.7, 161.8 (2), 149.5, 135.4, 128.5, 92.0 (2), 89.8, 59.4, 59.2, 55.3 (2), 54.4, 46.9, 45.5, 40.6, 35.1, 31.5, 28.0, 26.3, 24.9, 24.6, 24.1, 19.2. ESI-HRMS: calcd for $C_{25}H_{36}N_3O_3$ $[M + H]^+$: 426.2751, found: 426.2739.

*4.2.3.15. 12N-N′-(3,5-Ditrifluoromethylphenylamino)acetyl aloperine (**14o**)..* Yield 27%; white solid; m.p. 73–75 °C. ^{1}H NMR (400 MHz, $CDCl_3$) δ 7.16 (s, 1H), 6.94 (s, 2H), 5.67 (d, J = 5.2 Hz, 1H), 5.52 (s, 1H), 4.75 (d, J = 5.2 Hz, 1H), 4.04–3.95 (m, 1H), 3.90–3.73 (m, 2H), 3.48–3.39 (m, 1H), 3.10–3.01 (m, 1H), 2.75 (d, J = 7.6 Hz, 2H), 2.63–2.56 (m, 1H), 2.44 (s, 1H), 2.39–2.25 (m, 2H), 2.20–2.07 (m, 1H), 1.99 (s, 1H), 1.92–1.75 (m, 5H), 1.73–1.61 (m, 2H), 1.51–1.39 (m, 1H), 1.17–1.01 (m, 2H); ^{13}C NMR (101 MHz) δ 166.5, 147.9, 135.1, 132.5 (2), 128.8, 123.7 (2), 112.1, 110.2 (2), 59.5, 59.4, 54.4, 46.9, 44.8, 40.7, 35.1, 31.5, 28.0, 26.3, 24.9, 24.7, 24.0, 19.2. ESI-HRMS: calcd for $C_{25}H_{30}F_6N_3O$ $[M + H]^+$: 502.2288, found: 502.2276.

*4.2.3.16. 12 N-N′-(1-Naphthylamino)acetyl aloperine (**14p**)..* Yield 40%; white solid; m.p. 82–84 °C. ^{1}H NMR (500 MHz, $CDCl_3$) δ 8.06–7.97 (m, 1H), 7.83–7.75 (m, 1H), 7.50–7.42 (m, 2H), 7.34 (t, J = 7.5 Hz, 1H), 7.28–7.21 (m, 1H), 6.48 (d, J = 7.5 Hz, 1H), 5.96–5.85 (m, 1H), 5.67 (d, J = 5.0 Hz, 1H), 4.82 (d, J = 5.5 Hz, 1H), 4.20–4.09 (m, 1H), 4.04–3.96 (m, 1H), 3.84–3.74 (m, 1H), 3.57–3.46 (m, 1H), 3.15–3.03 (m, 1H), 2.81–2.69 (m, 2H), 2.66–2.54 (m, 1H), 2.50 (s, 1H), 2.43–2.37 (m, 1H), 2.33–2.22 (m, 1H), 2.20–2.10 (m, 1H), 2.02–1.62 (m, 8H), 1.51–1.37 (m, 1H), 1.17–1.03 (m, 2H); ^{13}C NMR (126 MHz) δ 167.9, 142.9, 135.4, 134.4, 128.5 (2), 126.6, 126.0, 124.9, 123.5, 120.6, 117.3, 104.0, 59.4 (2), 54.4, 46.9, 45.5, 40.6, 35.1, 31.6, 28.0, 26.3, 24.9, 24.6, 24.0, 19.2. ESI-HRMS: calcd for $C_{27}H_{34}N_3O$ $[M + H]^+$: 416.2696, found: 416.2688.

*4.2.3.17. 12N-N′-(2-Naphthylamino)acetyl aloperine (**14q**)..* Yield 43%; white solid; m.p. 84–86 °C. ^{1}H NMR (500 MHz, $CDCl_3$) δ 7.68 (d, J = 8.5 Hz, 1H), 7.63 (t, J = 8.5 Hz, 2H), 7.40–7.33 (m, 1H), 7.20 (t, J = 7.5 Hz, 1H), 6.99 (dd, J = 8.5, 2.0 Hz, 1H), 6.75–6.68 (m, 1H), 5.66 (d, J = 5.5 Hz, 1H), 5.23–5.16 (m, 1H), 4.79 (d, J = 5.5 Hz, 1H), 4.16–4.04 (m, 1H), 3.99–3.91 (m, 1H), 3.86–3.74 (m, 1H), 3.56–3.47 (m, 1H), 3.15–3.02 (m, 1H), 2.81–2.70 (m, 2H), 2.66–2.52 (m, 1H), 2.47 (s, 1H), 2.41–2.35 (m, 1H), 2.33–2.23 (m, 1H), 2.19–2.09 (m, 1H), 2.02–1.76 (m, 6H), 1.74–1.61 (m, 2H), 1.51–1.38 (m, 1H), 1.15–1.03 (m, 2H); ^{13}C NMR (126 MHz) δ 167.7, 145.2, 135.4, 135.3, 129.1, 128.5, 127.8, 127.6, 126.4, 125.9, 122.0, 118.5, 104.0, 59.4, 59.3, 54.4, 46.9, 45.4, 40.6, 35.1, 31.5, 28.0, 26.3, 24.9, 24.7, 24.0, 19.2. ESI-HRMS: calcd for $C_{27}H_{34}N_3O$ $[M + H]^+$: 416.2696, found: 416.2685.

4.2.3.18. 12N-N′-Methyl-N′-p-chlorophenyl aminoacetylaloperine (14r).. Yield 38%; white solid; m.p. 54–56 °C. ^{1}H NMR (600 MHz, $CDCl_3$) δ 7.16–7.12 (m, 2H), 6.60 (d, J = 8.4 Hz, 2H), 5.62 (d, J = 3.6 Hz, 1H), 4.70 (s, 1H), 4.18–4.00 (m, 2H), 3.78–3.61 (m, 1H), 3.52–3.38 (m, 1H), 3.04 (s, 4H), 2.78–2.68 (m, 2H), 2.62–2.53 (m, 1H), 2.46–2.29 (m, 2H), 2.29–2.19 (m, 1H), 2.15–2.05 (m, 1H), 1.98–1.79 (m, 5H), 1.76–1.59 (m, 3H), 1.49–1.39 (m, 1H), 1.17–1.01 (m, 2H); ^{13}C NMR (151 MHz) δ 168.3, 148.4, 135.7, 129.1 (3), 128.3, 122.1, 113.8, 59.6, 59.2, 54.9, 54.5, 47.0, 41.2, 40.0, 35.2, 31.5, 28.1, 26.3, 25.1, 24.9, 24.2, 19.4. ESI-HRMS: calcd for $C_{24}H_{33}ClN_3O$ $[M + H]^+$: 414.2307, found: 414.2311.

*4.2.4. General procedures for the synthesis of 12 N-carbamoyl aloperines (**15a–d**)*

To a solution of aloperine (2 mmol) in anhydrous CH_2Cl_2 (30 mL) at 0 °C, after the addition of triethylamine (2.4 mmol), the different substituted isocyanates (2 mmol) were respectively added slowly. After 30 min, reaction was warmed to r.t. and stirred for 0.5 h. The gained mixture was concentrated to give a residue, which was purified by flash column chromatography on silica gel with CH_2Cl_2/CH_3OH as the eluent to get the title compounds **15a**–**d**.

*4.2.4.1. 12N-N′-(2,4-Difluorophenyl)carbamoyl aloperine (**15a**)..* Yield 26%; white solid; m.p. 168–170 °C. ^{1}H NMR (500 MHz, $CDCl_3$) δ 8.15–8.05 (m, 1H), 6.88–6.79 (m, 2H), 6.45 (s, 1H), 5.64 (s, 1H), 4.48 (s, 1H), 3.80–3.69 (m, 1H), 3.63–3.52 (m, 1H), 3.15–3.04 (m, 1H), 2.82–2.66 (m, 2H), 2.6–2.53 (m, 2H), 2.33–2.25 (m, 2H), 2.18–2.12 (m, 1H), 2.03–1.80 (m, 5H), 1.72–1.63 (m, 3H), 1.52–1.37 (m, 1H), 1.17–1.02 (m, 2H). ^{13}C NMR (126 MHz) δ 156.0, 154.8, 154.1, 135.9, 128.2, 124.4, 122.5, 111.2, 103.4, 59.9, 59.6, 54.4, 46.7, 40.3, 35.1, 33.4, 28.4, 26.3, 25.1, 24.3 (2), 19.5. ESI-HRMS: calcd for $C_{22}H_{28}F_2N_3O$ $[M + H]^+$: 388.2195, found: 388.2193.

*4.2.4.2. 12N-N′-(3,5-Dimethylphenyl)carbamoyl aloperine (**15b**)..* Yield

63%; white solid; m.p. 106–108 °C. ^{1}H NMR (600 MHz, $CDCl_3$) δ 7.06 (s, 2H), 6.65 (s, 1H), 6.23 (s, 1H), 5.61 (d, J = 4.9 Hz, 1H), 4.49 (d, J = 4.8 Hz, 1H), 3.72 (dd, J = 13.4, 6.4 Hz, 1H), 3.58–3.53 (m, 1H), 3.07 (dd, J = 11.6, 3.6 Hz, 1H), 2.78 (d, J = 13.3 Hz, 1H), 2.74–2.69 (m, 1H), 2.58–2.55 (m, 2H), 2.31 (s, 1H), 2.27 (s, 6H), 2.24 (d, J = 11.2 Hz, 1H), 2.17–2.12 (m, 1H), 2.02–1.98 (m, 2H), 1.91 (d, J = 12.7 Hz, 1H), 1.87–1.79 (m, 2H), 1.71–1.66 (m, 3H), 1.48–1.40 (m, 1H), 1.12 (d, J = 13.2 Hz, 1H), 1.08 (d, J = 13.4 Hz, 1H); ^{13}C NMR (151 MHz) δ 155.1, 139.2, 138.5 (2), 136.0, 127.6, 124.4, 117.2 (2), 59.5 (2), 54.2, 46.6, 40.0, 35.0, 33.3, 28.3, 26.1, 24.9, 24.3, 24.2, 21.4 (2), 19.3. ESI-HRMS: calcd for $C_{24}H_{34}N_3O$ $[M + H]^+$: 380.2696, found: 380.2692.

*4.2.4.3. 12N-N′-(3,5-Ditrifluoromethylphenyl)carbamoyl aloperine (**15c**).*. Yield 46%; white solid; m.p. 134–136 °C. ^{1}H NMR (400 MHz, $CDCl_3$) δ 7.95 (s, 2H), 7.48 (s, 1H), 6.66 (s, 1H), 5.66 (d, J = 4.4 Hz, 1H), 4.53 (s, 1H), 3.76–3.62 (m, 2H), 3.18–3.07 (m, 1H), 2.86–2.48 (m, 3H), 2.37–2.24 (m, 2H), 2.22–2.10 (m, 1H), 2.05–1.99 (m, 1H), 1.99–1.91 (m, 2H), 1.91–1.82 (m, 2H), 1.76–1.61 (m, 4H), 1.52–1.37 (m, 1H), 1.21–1.01 (m, 2H); ^{13}C NMR (151 MHz, DMSO-d_6) δ 154.1, 142.9, 135.8, 130.2 (2), 127.0, 123.4 (2), 118.9, 118.8, 113.6, 58.7, 58.3, 54.8, 53.6, 46.0, 34.4, 31.9, 27.6, 25.6, 24.4, 24.0, 23.4, 18.7. ESI-HRMS: calcd for $C_{24}H_{28}F_6N_3O$ $[M + H]^+$: 488.2131, found: 488.2122.

*4.2.4.4. 12N-N′-(1-Adamanty)carbamoyl aloperine (**15d**).*. Yield 57%; white solid; m.p. 99–101 °C. ^{1}H NMR (400 MHz, $CDCl_3$) δ 5.55 (d, J = 4.8 Hz, 1H), 4.28 (d, J = 5.2 Hz, 1H), 4.09 (s, 1H), 3.64–3.52 (m, 1H), 3.41–3.29 (m, 1H), 3.08–2.98 (m, 1H), 2.83–2.63 (m, 2H), 2.59–2.48 (m, 1H), 2.28–2.16 (m, 2H), 2.14–2.01 (m, 5H), 1.99–1.96 (m, 5H), 1.95–1.92 (m, 1H), 1.91–1.76 (m, 3H), 1.71–1.68 (m, 2H), 1.68–1.57 (m, 9H), 1.44–1.38 (m, 1H), 1.18–1.03 (m, 2H); ^{13}C NMR (101 MHz) δ 157.2, 136.8, 127.1, 59.9, 59.2, 54.4, 51.2, 46.8, 44.8, 42.8 (2), 42.7, 36.7 (2), 36.2, 35.1, 33.3, 29.8 (2), 29.7, 28.6, 26.1, 24.8, 24.7, 24.3, 19.7. ESI-HRMS: calcd for $C_{26}H_{40}N_3O$ $[M + H]^+$: 410.3166, found: 410.3153.

4.3. Biological evaluation

4.3.1. Cell culture

HEK 293 T (American Type Culture Collection (ATCC), CRL-3216), Huh 7 (Japanese Collection of Research Bioresources [JCRB], 0403) and Vero E6 (ATCC, CRL-1586) cells were cultured in Dulbecco's modified Eagle's medium (HyClone, South Logan, UT). The medium was supplemented with 10% fetal bovine serum (Gibco, Carlsbad, CA, USA), 1% penicillin–streptomycin solution (Gibco, Carlsbad, CA, USA), 2% 4-(2-hydroxy ethyl)-1-piperazineethanesulfonic acid (Gibco, Carlsbad, CA, USA) at 37 °C with 5% CO_2.

4.3.2. Pseudotyped virus

The monolayer 293 T cells were cotransfected with plasmid pcDNA3.1.S2 using lipofectamine 3000 (Invitrogen, Carlsbad, CA), and G*ΔG-VSV were added [28]. After incubated for 6 h, the medium was replaced with fresh medium and incubated for 24 h. The culture supernatants containing the pseudovirus were harvested, filtered (0.45 μM pore-size) and stored in 1 mL aliquots at –80 °C until use. 50% tissue culture infectious dose ($TCID_{50}$) of pseudoviruses was determined as described previously [28]. All works involving pseudotyped viruses were performed in a BSL-2 facility at the National Institutes of Food and Drug Control (NIFDC), Beijing, China.

4.3.3. In vitro screening assay with pseudoviruses

For primary screening, serial dilutions (starting from 1:150) of each compound (30 mM) were mixed with 1.3 × 10^4 $TCID_{50}$ of SARS-CoV-2 pseudovirus in 96-well Costar plates (Corning, Inc., Corning, NY) at 37 °C for 1 h, then mixed with Huh 7 cells (2 × 10^4 cells/well) and subsequently incubated for 24 h. The infectivity was determined by measuring the bioluminescence as described previously based on neutralization assay. The EC_{50} was determined from the dose–response curve, and cytotoxicity testing was performed to determine the CC_{50} of each test compound in the absence of pseudovirus.

4.3.4. Evaluation of key compounds with authentic SARS-CoV-2 in BSL-3

Serial dilutions of compounds **2e**, **8a** and **8b** (30 mM) were mixed with 0.1 MOI authentic SARS-CoV-2 in 96-well Costar plates at 37 °C for 1 h, then Vero E6 cells (2 × 10^4 cells/well) were added and subsequently incubated for 3 days. EC_{50} of each compound were determined by CPE assay. Cytotoxicity testing was performed to determine the CC_{50} of each test compound in Vero E6 cells.

4.4. Time-of-addition experiment

The time of addition experiment of compounds **8a** and CA-074 was performed to on SARS-CoV-2 pseudovirus. Huh 7 cells were pre-packaged in 96-well plates 1 day in advance. Then 25 μM concentration of the compounds were added at during pseudovirus infection at 37 °C (**a** process), or at 0 °C (**b** process), and 1 h before pseudovirus infection (**c** process), and 1 h post infection (**d** process) at different temperature. After incubated at 37 °C for another 23 h, the inhibition rate was determined by measuring the bioluminescence as described previously [28].

4.5. Cathepsins activity assay

Cat B activity was assayed using the Cat B substrate *N*-benzyloxycarbonyl- L-arginyl-L-arginine-7-amido-4-methylcoumarin (Calbiochem) in cell lysates adjusted to pH of 5.0, as described previously [23]. Cat L activity was assayed in the same process as Cat B, but the Cat L substrate was *N*-benzyloxycarbonyl-L-phenyl alanyl-L-arginine-7-amido-4-methylcoumarin (Calbiochem).

4.6. PK study

Male SD rats were received 25 mg/kg with the compound **8a** via oral administration. Nine blood samples were sequentially collected at 0.25, 0.5, 1.0, 2.0, 4.0, 6.0, 8.0, 12 and 24 h after the dose, and immediately centrifuged to separate the plasma fractions at 10000 rpm for 10 min. The separated plasma samples were stored at –20 °C for assay. Non-compartmental PK analysis was performed on the serum concentration-versus-time profile of **8a** derived from each SD rat with a nonlinear regression curve fitting program WinNonlin software, version 5.3.

4.7. Safety assessments

Kunming mice with weighting of 20 g ± 1.0 g were purchased from the Beijing HFK Biosciences Co. LTD. The mice were fed with a regular rodent diet and housed according to the guidelines of the CAMS & PUMC. After 3 days of accommodation, mice were randomly divided into 4 groups with 6 mice each, and compound **8a** was given orally in a single-dosing experiment at 0, 250, 500 or 1000 mg•kg^{-1} (saline as control), respectively. The survival and body weight of the mice were closely monitored for 7 days. Seven days later, blood samples were collected and serum were isolated for determination of ALT, AST, BUN, and SCR levels.

Declaration of Competing Interest

The authors declare that they have no known competing financial interests or personal relationships that could have appeared to influence the work reported in this paper.

Acknowledgements

This work was supported by the National Natural Science Foundation of China (81974494), the CAMS Innovation Fund for Medical Sciences (2020-I2M-2-010 and 2016–I2M–3–009) and Graduate Innovation Fund for Peking Union Medical College (2019–1007–20).

Appendix A. Supplementary data

Supplementary data to this article can be found online at https://doi.org/10.1016/j.bioorg.2021.105196.

References

[1] V. Coronaviridae Study Group of the International Committee on Taxonomy of, The species Severe acute respiratory syndrome-related coronavirus: classifying 2019-nCoV and naming it SARS-CoV-2, Nat. Microbiol. 5 (2020) 536–544.
[2] World Health Organization, WHO Coronavirus Disease (COVID-19) Dashboard. https://covid19.who.int, 2020 (accessed 13 December 2020).
[3] Manli Wang, Ruiyuan Cao, Leike Zhang, Xinglou Yang, Jia Liu, Mingyue Xu, Zhengli Shi, Zhihong Hu, Wu Zhong, Gengfu Xiao, Remdesivir and chloroquine effectively inhibit the recently emerged novel coronavirus (2019-nCoV) in vitro, Cell Res. 30 (3) (2020) 269–271.
[4] M.L. Holshue, C. DeBolt, S. Lindquist, K.H. Lofy, J. Wiesman, H. Bruce, C. Spitters, K. Ericson, S. Wilkerson, A. Tural, G. Diaz, A. Cohn, L. Fox, A. Patel, S.I. Gerber, L. Kim, S. Tong, X. Lu, S. Lindstrom, M.A. Pallansch, W.C. Weldon, H.M. Biggs, T. M. Uyeki, S.K. Pillai, First Case of 2019 Novel Coronavirus in the United States, N. Engl. J. Med. 382 (2020) (2019) 929–936.
[5] Xueting Yao, Fei Ye, Miao Zhang, Cheng Cui, Baoying Huang, Peihua Niu, Xu Liu, Li Zhao, Erdan Dong, Chunli Song, Siyan Zhan, Roujian Lu, Haiyan Li, Wenjie Tan, Dongyang Liu, In vitro antiviral activity and projection of optimized dosing design of hydroxychloroquine for the treatment of Severe Acute Respiratory Syndrome Coronavirus 2 (SARS-CoV-2), Clin. Infect. Dis. 71 (15) (2020) 732–739.
[6] P. Colson, J.M. Rolain, J.C. Lagier, P. Brouqui, D. Raoult, Chloroquine and hydroxy chloroquine as available weapons to fight COVID-19, Int. J. Antimicrob. Agents 55 (2020), 105932.
[7] Mário Luciano de Mélo Silva Júnior, Lívia Maria Alves de Souza, Renata Ellen Maria Carvalho Dutra, Ramon Gonçalves de Melo Valente, Thayanara Silva Melo, Review on therapeutic targets for COVID-19: insights from cytokine storm, Postgrad Med J. 97 (1148) (2021) 391–398, https://doi.org/10.1136/postgradmedj-2020-138791.
[8] M.R. Mehra, S.S. Desai, F. Ruschitzka, A.N. Patel, Hydroxychloroquine or chloroquine with or without a macrolide for treatment of COVID-19: a multinational registry analysis, Lancet S 0140–6736 (2020) 31180–31186.
[9] M.G.S. Borba, F.F.A. Val, V.S. Sampaio, M.A.A. Alexandre, G.C. Melo, M. Brito, M. P.G. Mourao, J.D. Brito-Sousa, D. Baia-da-Silva, M.V.F. Guerra, L.A. Hajjar, R. C. Pinto, A.A.S. Balieiro, A.G.F. Pacheco, J.D.O. Santos Jr., F.G. Naveca, M. S. Xavier, A.M. Siqueira, A. Schwarzbold, J. Croda, M.L. Nogueira, G.A.S. Romero, Q. Bassat, C.J. Fontes, B.C. Albuquerque, C.T. Daniel-Ribeiro, W.M. Monteiro, M.V. G. Lacerda, T. CloroCovid, Effect of high vs low doses of chloroquine diphosphate as adjunctive therapy for patients hospitalized with severe acute respiratory syndrome coronavirus 2 (SARS-CoV-2) infection: a randomized clinical trial, JAMA. Netw. Open 3 (2020), e208857.
[10] A.B. Cavalcanti, F.G. Zampieri, R.G. Rosa, L.C.P. Azevedo, V.C. Veiga, A. Avezum, L.P. Damiani, A. Marcadenti, L. Kawano-Dourado, T. Lisboa, D.L.M. Junqueira, E.S. P.G.M. de Barros, L. Tramujas, E.O. Abreu-Silva, L.N. Laranjeira, A.T. Soares, L. S. Echenique, A.J. Pereira, F.G.R. Freitas, O.C.E. Gebara, V.C.S. Dantas, R.H. M. Furtado, E.P. Milan, N.A. Golin, F.F. Cardoso, I.S. Maia, C.R. Hoffmann Filho, A. P.M. Kormann, R.B. Amazonas, M.F. Bocchi de Oliveira, A. Serpa-Neto, M. Falavigna, R.D. Lopes, F.R. Machado, O. Berwanger, I.I. Coalition, Covid-19 Brazil, Hydroxychloroquine with or without azithromycin in mild-to-moderate covid-19, N. Engl. J. Med. 383 (2020) 2041–2052.
[11] Bin Cao, Yeming Wang, Danning Wen, Wen Liu, Jingli Wang, Guohui Fan, Lianguo Ruan, Bin Song, Yanping Cai, Ming Wei, Xingwang Li, Jiaan Xia, Nanshan Chen, Jie Xiang, Ting Yu, Tao Bai, Xuelei Xie, Li Zhang, Caihong Li, Ye Yuan, Hua Chen, Huadong Li, Hanping Huang, Shengjing Tu, Fengyun Gong, Ying Liu, Yuan Wei, Chongya Dong, Fei Zhou, Xiaoying Gu, Jiuyang Xu, Zhibo Liu, Yi Zhang, Hui Li, Lianhan Shang, Ke Wang, Kunxia Li, Xia Zhou, Xuan Dong, Zhaohui Qu, Sixia Lu, Xujuan Hu, Shunan Ruan, Shanshan Luo, Jing Wu, Lu Peng, Fang Cheng, Lihong Pan, Jun Zou, Chunmin Jia, Juan Wang, Xia Liu, Shuzhen Wang, Xudong Wu, Qin Ge, Jing He, Haiyan Zhan, Fang Qiu, Li Guo, Chaolin Huang, Thomas Jaki, Frederick G. Hayden, Peter W. Horby, Dingyu Zhang, Chen Wang, A trial of Lopinavir-Ritonavir in adults hospitalized with severe covid-19, N. Engl. J. Med. 382 (19) (2020) 1787–1799.
[12] John H. Beigel, Kay M. Tomashek, Lori E. Dodd, Aneesh K. Mehta, Barry S. Zingman, Andre C. Kalil, Elizabeth Hohmann, Helen Y. Chu, Annie Luetkemeyer, Susan Kline, Diego Lopez de Castilla, Robert W. Finberg, Kerry Dierberg, Victor Tapson, Lanny Hsieh, Thomas F. Patterson, Roger Paredes, Daniel A. Sweeney, William R. Short, Giota Touloumi, David Chien Lye, Norio Ohmagari, Myoung-don Oh, Guillermo M. Ruiz-Palacios, Thomas Benfield, Gerd Fätkenheuer, Mark G. Kortepeter, Robert L. Atmar, C. Buddy Creech, Jens Lundgren, Abdel G. Babiker, Sarah Pett, James D. Neaton, Timothy H. Burgess, Tyler Bonnett, Michelle Green, Mat Makowski, Anu Osinusi, Seema Nayak, H. Clifford Lane, ACTT-1 Study Group Members, Remdesivir for the treatment of Covid-19-final report, N. Engl. J. Med. 383 (19) (2020) 1813–1826.
[13] Y. Wang, D. Zhang, G. Du, R. Du, J. Zhao, Y. Jin, S. Fu, L. Gao, Z. Cheng, Q. Lu, Y. Hu, G. Luo, K. Wang, Y. Lu, H. Li, S. Wang, S. Ruan, C. Yang, C. Mei, Y. Wang, D. Ding, F. Wu, X. Tang, X. Ye, Y. Ye, B. Liu, J. Yang, W. Yin, A. Wang, G. Fan, F. Zhou, Z. Liu, X. Gu, J. Xu, L. Shang, Y. Zhang, L. Cao, T. Guo, Y. Wan, H. Qin, Y. Jiang, T. Jaki, F.G. Hayden, P.W. Horby, B. Cao, C. Wang, Remdesivir in adults with severe COVID-19: a randomised, double-blind, placebo-controlled, multicentre trial, Lancet 395 (2020) 1569–1578.
[14] The US Food and Drug Administration, FDA's approval of Veklury (remdesivir) for the treatment of COVID-19—The Science of Safety and Effectiveness. https://www.fda.gov /drugs/drug-safety-and-availability/fdas-approval-veklury-remdesivir-treatment-covid-19-science-safety-and-effectiveness, 2020 (accessed 13 December 2020).
[15] J.A. Plante, Y. Liu, J. Liu, H. Xia, B.A. Johnson, K.G. Lokugamage, X. Zhang, A. E. Muruato, J. Zou, C.R. Fontes-Garfias, D. Mirchandani, D. Scharton, J.P. Bilello, Z. Ku, Z. An, B. Kalveram, A.N. Freiberg, V.D. Menachery, X. Xie, K.S. Plante, S. C. Weaver, P.Y. Shi, Spike mutation D614G alters SARS-CoV-2 fitness, Nature 592 (7852) (2021) 116–121, https://doi.org/10.1038/s41586- 020-2895-3.
[16] B. Korber, W.M. Fischer, S. Gnanakaran, H. Yoon, J. Theiler, W. Abfalterer, N. Hengartner, E.E. Giorgi, T. Bhattacharya, B. Foley, K.M. Hastie, M.D. Parker, D. G. Partridge, C.M. Evans, T.M. Freeman, T.I. de Silva, C.-G.G. Sheffield, C. McDanal, L.G. Perez, H. Tang, A. Moon-Walker, S.P. Whelan, C.C. LaBranche, E. O. Saphire, D.C. Montefiori, Tracking changes in SARS-CoV-2 spike: evidence that D614G increases infectivity of the COVID-19 virus, Cell 182 (2020) 812–827.
[17] Qianqian Li, Jiajing Wu, Jianhui Nie, Li Zhang, Huan Hao, Shuo Liu, Chenyan Zhao, Qi Zhang, Huan Liu, Lingling Nie, Haiyang Qin, Meng Wang, Qiong Lu, Xiaoyu Li, Qiyu Sun, Junkai Liu, Linqi Zhang, Xuguang Li, Weijin Huang, Youchun Wang, The impact of mutations in SARS-CoV-2 spike on viral infectivity and antigenicity, Cell 182 (5) (2020) 1284–1294.e9.
[18] K.K. To, I.F. Hung, J.D. Ip, A.W. Chu, W.M. Chan, A.R. Tam, C.H. Fong, S. Yuan, H. W. Tsoi, A.C. Ng, L.L. Lee, P. Wan, E. Tso, W.K. To, D. Tsang, K.H. Chan, J. D. Huang, K.H. Kok, V.C. Cheng, K.Y. Yuen, COVID-19 re-infection by a phylogenetically distinct SARS- coronavirus-2 strain confirmed by whole genome sequencing, Clin. Infect. Dis. (2020) ciaa1275.
[19] Michelangelo Luciani, Enrico Bentivegna, Valerio Spuntarelli, Piera Amoriello Lamberti, Giulio Cacioli, Flavia Del Porto, Giorgio Sesti, Paolo Martelletti, Luciano De Biase, Recurrent Covid-19 pneumonia in the course of chemotherapy: consequence of a weakened immune system? J. Med. Virol. 93 (4) (2021) 1882–1884, https://doi.org/10.1002/jmv.v93.410.1002/jmv.26701.
[20] Peipei Song, Wei Li, Jianqin Xie, Yanlong Hou, Chongge You, Cytokine storm induced by SARS-CoV-2, Clin. Chim. acta 509 (2020) 280–287.
[21] B. Hu, S. Huang, L. Yin, The cytokine storm and COVID-19, J. Med. Virol. (2020), 10.1002/ jmv.26232.
[22] R.C. Group, P. Horby, W.S. Lim, J.R. Emberson, M. Mafham, J.L. Bell, L. Linsell, N. Staplin, C. Brightling, A. Ustianowski, E. Elmahi, B. Prudon, C. Green, T. Felton, D. Chadwick, K. Rege, C. Fegan, L.C. Chappell, S.N. Faust, T. Jaki, K. Jeffery, A. Montgomery, K. Rowan, E. Juszczak, J.K. Baillie, R. Haynes, M.J. Landray, Dexamethasone in hospitalized patients with Covid-19-preliminary report, N. Engl. J. Med. (2020). NEJMoa 2021436.
[23] Xin Zhang, Qiang Liu, Na Zhang, Qian–Qian Li, Zhan–Dong Liu, Ying–Hong Li, Li–Mei Gao, You–Chun Wang, Hong–Bin Deng, Dan–Qing Song, Discovery and evolution of aloperine derivatives as novel anti-filovirus agents through targeting entry stage, Eur. J. Med. Chem. 149 (2018) 45–55.
[24] Xin Zhang, Xiao–Qin Lv, Sheng Tang, Lin Mei, Ying–Hong Li, Jing–Pu Zhang, Jian–Dong Jiang, Zong–Gen Peng, Dan–Qing Song, Discovery and evolution of aloperine derivatives as a new family of HCV inhibitors with novel mechanism, Eur. J. Med. Chem. 143 (2018) 1053–1065.
[25] Xin Zhang, Qiang Liu, Qianqian Li, Yinghong Li, Zhandong Liu, Hongbin Deng, Sheng Tang, Yanxiang Wang, Youchun Wang, Danqing Song, Synthesis and biological evaluation of novel tricyclic matrinic derivatives as potential anti-filovirus agents, Acta Pharm. Sin. B 8 (4) (2018) 629–638.
[26] Li Zhang, Qianqian Li, Qiang Liu, Weijin Huang, Jianhui Nie, Youchun Wang, A bioluminescent imaging mouse model for Marburg virus based on a pseudovirus system, Hum. Vaccin. immunother. 13 (8) (2017) 1811–1817.
[27] Q. Liu, C. Fan, Q. Li, S. Zhou, W. Huang, L. Wang, C. Sun, M. Wang, X. Wu, J. Ma, B. Li, L. Xie, Y. Wang, Antibody-dependent-cellular-cytotoxicity-inducing antibodies significantly affect the post-exposure treatment of Ebola virus infection, Sci. Rep. 7 (2017) 45552.
[28] Jianhui Nie, Qianqian Li, Jiajing Wu, Chenyan Zhao, Huan Hao, Huan Liu, Li Zhang, Lingling Nie, Haiyang Qin, Meng Wang, Qiong Lu, Xiaoyu Li, Qiyu Sun, Junkai Liu, Changfa Fan, Weijin Huang, Miao Xu, Youchun Wang, Establishment and validation of a pseudovirus neutralization assay for SARS-CoV-2, Emerg. Microbes Infect. 9 (1) (2020) 680–686.
[29] Jianhui Nie, Qianqian Li, Jiajing Wu, Chenyan Zhao, Huan Hao, Huan Liu, Li Zhang, Lingling Nie, Haiyang Qin, Meng Wang, Qiong Lu, Xiaoyu Li, Qiyu Sun, Junkai Liu, Changfa Fan, Weijin Huang, Miao Xu, Youchun Wang, Quantification of SARS-CoV-2 neutralizing antibody by a pseudotyped virus-based assay, Nat. protoc. 15 (11) (2020) 3699–3715.
[30] K. Wang, Z. Guo, Y. Bao, Y. Pang, Y. Li, H. He, D. Song, Structure-activity relationship of aloperine derivatives as new anti-liver fibrogenic agents, Molecules 25 (2020) 4977.
[31] C. Fan, X. Wu, Q. Liu, Q. Li, S. Liu, J. Lu, Y. Yang, Y. Cao, W. Huang, C. Liang, T. Ying, S. Jiang, Y. Wang, A human DPP4-Knockin mouse's susceptibility to infection by authentic and pseudotyped MERS-CoV, Viruses 10 (2018) 448.

[32] Markus Hoffmann, Hannah Kleine-Weber, Simon Schroeder, Nadine Krüger, Tanja Herrler, Sandra Erichsen, Tobias S. Schiergens, Georg Herrler, Nai-Huei Wu, Andreas Nitsche, Marcel A. Müller, Christian Drosten, Stefan Pöhlmann, SARS-CoV-2 cell entry depends on ACE2 and TMPRSS2 and is blocked by a clinically proven protease inhibitor, Cell 181 (2) (2020) 271–280.e8.

[33] T. Tang, M. Bidon, J.A. Jaimes, G.R. Whittaker, S. Daniel, Coronavirus membrane fusion mechanism offers a potential target for antiviral development, Antiviral Res. 178 (2020), 104792.

[34] X. Ou, Y. Liu, X. Lei, P. Li, D. Mi, L. Ren, L. Guo, R. Guo, T. Chen, J. Hu, Z. Xiang, Z. Mu, X. Chen, J. Chen, K. Hu, Q. Jin, J. Wang, Z. Qian, Characterization of spike glycoprotein of SARS-CoV-2 on virus entry and its immune cross-reactivity with SARS-CoV, Nat. Commun. 11 (2020) 1620.

[35] Jian Shang, Yushun Wan, Chuming Luo, Gang Ye, Qibin Geng, Ashley Auerbach, Fang Li, Cell entry mechanisms of SARS-CoV-2, Proc. Natl. Acad. Sci. U. S. A. 117 (21) (2020) 11727–11734.

[36] C.S.B. da Silva, M. Thaler, A. Tas, N.S. Ogando, P.J. Bredenbeek, D.K. Ninaber, Y. Wang, P.S. Hiemstra, E.J. Snijder, M.J. van Hemert, Suramin inhibits SARS-CoV-2 infection in cell culture by interfering with early steps of the replication cycle, Antimicrob. Agents Chemother. 64 (2020) e00900–e920.

[37] Charles J. Shoemaker, Kathryn L. Schornberg, Sue E. Delos, Corinne Scully, Hassan Pajouhesh, Gene G. Olinger, Lisa M. Johansen, Judith M. White, Lijun Rong, Multiple cationic amphiphiles induce a Niemann-Pick C phenotype and inhibit Ebola virus entry and infection, PLoS One 8 (2) (2013) e56265, https://doi.org/10.1371/journal.pone.0056265.

[38] Yi-Nan Gong, Xiaoming Wang, Jiayi Wang, Zhenxiao Yang, Shan Li, Jieling Yang, Liping Liu, Xiaoguang Lei, Feng Shao, Chemical probing reveals insights into the signaling mechanism of inflammasome activation, Cell Res. 20 (12) (2010) 1289–1305.